https://doi.org/10.5194/egusphere-2026-5134
Preprint. Discussion started: 8 September 2026

Quantifying parameter-induced uncertainty and evaluating the effects of model simplification in a marine biogeochemical model

Yutong Zhang[1], Pierre Brasseur[2], Melika Baklouti[1], and Jean-Michel Brankart[2]

[1]Aix-Marseille Université, Université de Toulon, CNRS, IRD, MIO UM 110, Campus de Luminy – OCEANOMED, 13288 Marseille CEDEX 09, France
[2]CNRS, INRAE, IRD, Grenoble INP, IGE, Université Grenoble Alpes, 38400 Saint-Martin-d'Hères, France

Correspondence: Yutong Zhang (yutong.zhang@univ-amu.fr)

Abstract. Marine biogeochemical models are widely used to investigate plankton ecosystem dynamics and biogeochemical cycling. However, their increasing complexity makes large ensemble analyses of parameter-induced uncertainty computationally demanding. Model simplification can reduce computational cost, but it may also modify how parameter perturbations propagate through ecological and biogeochemical processes. This study examines whether model simplification affects not only mean-state behaviour, but also the magnitude and time-depth distribution of parameter-induced uncertainty. We used the one-dimensional vertical configuration of the Eco3M-MED-V1b model at the DYFAMED station in the northwestern Mediterranean Sea, and compared the full-complexity (FULL) version with two simplified versions: MOD1, designed to preserve the state variables, and MOD2, designed to preserve a set of key ecosystem indicators. A common 512-member Sobol low-discrepancy ensemble was generated by perturbing 30 parameters shared by the three model versions, allowing direct comparison under identical parameter perturbations. The results show that parameter-induced uncertainty in FULL is concentrated in ecologically important periods and depths, including the upper productive layer, near the nutricline, the deep chlorophyll maximum, and during the spring bloom and summer stratification. Model simplification did not systematically increase or decrease uncertainty; instead, its effects varied among variables, ecosystem indicators, periods and depths. MOD1 broadly preserved the main time–depth distribution of uncertainty in the state variables, whereas MOD2 generally preserved the uncertainty magnitude of most ecosystem indicators. However, similar uncertainty magnitudes in indicators integrated over the whole year or water column may mask local differences occurring during specific periods or within specific depth ranges. Diagnostics used to guide model evaluation or simplification should therefore be defined *a priori* according to the scientific question and intended application. Uncertainty analysis can also help identify complementary diagnostics.

1 Introduction

Marine biogeochemical (BGC) models, especially when coupled with atmospheric and ocean circulation models, have become essential tools for studying marine ecosystems, including plankton food-web dynamics and major biogeochemical cycles (e.g. Moore et al., 2013; Lazzari et al., 2014; Aumont et al., 2015; Pagès et al., 2020). They are also widely used to simulate long-term ecosystem trajectories under IPCC SSP–RCP/Scenario climate pathways (Bopp et al., 2013; O'Neill et al., 2016;

https://doi.org/10.5194/egusphere-2026-5134
Preprint. Discussion started: 8 September 2026

Riahi et al., 2017; IPCC, 2023). In addition, marine BGC model outputs provide lower-trophic-level forcing (e.g. zooplankton biomass fields) for high-trophic-level and fisheries models (e.g. Rose et al., 2010; Morell et al., 2023; Eddy et al., 2025).

As our understanding of marine ecosystems has improved and more biogeochemical processes have been incorporated, BGC models have become increasingly complex in both structure and formulation (Leles et al., 2016). Model structures have progressively evolved from NPZ to NPZD (e.g. Fasham et al., 1990), and further towards models based on Phytoplankton Functional Types (PFTs) (e.g. Quéré et al., 2005; Baklouti et al., 2006). This increase in complexity has substantially enlarged the number of state variables and parameters, and therefore the computational cost (Ward et al., 2013; Anugerahanti et al., 2018). As a result, two major tasks are often difficult to achieve in practice: exploring large ensembles of long-term scenarios and carrying out model uncertainty quantification (UQ) and sensitivity analysis, both of which require many computationally expensive simulations. The main focus of this study is to quantify the parameter-induced uncertainty and explore how model simplification modifies these uncertainties.

Model simplification offers a practical way to make complex marine BGC models more tractable for these applications. Several studies have explored simplification strategies for marine BGC models (e.g. Raick et al., 2006; Ward et al., 2013; Jordan et al., 2025; Zhang et al., 2026), showing that reduced-complexity model versions can lower computational cost and make large ensemble simulations more feasible. However, by modifying model structure and the representation of ecological and biogeochemical processes, simplification may also change how parameter perturbations propagate to model outputs, including biomass, nutrient distributions, oxygen dynamics, and carbon export (Anugerahanti et al., 2018; Wang and Fennel, 2024). This issue is consistent with broader discussions in environmental and ecological modelling, in which model structure is recognised as an important source of uncertainty (Refsgaard et al., 2006, 2007; Turley and Ford, 2009). In practice, simplified models are still commonly evaluated mainly in terms of computational efficiency and their fidelity to a reference simulation. By contrast, the effects of simplification on parameter-induced uncertainty remain less explored, particularly regarding changes in its magnitude, its spatio-temporal distribution, as well as which model outputs are most affected.

Parameter-induced uncertainty is widely recognised as a major source of uncertainty in BGC models, as these models often involve many parameters (Schartau et al., 2017; Mamnun et al., 2023). In recent years, studies of parameter-induced uncertainty in BGC models have frequently relied on variance-based global sensitivity analysis methods, such as Sobol indices and eFAST, to identify influential parameters and estimate uncertainty ranges (e.g. Prieur et al., 2019; Löptien et al., 2021; Mamnun et al., 2023). However, in high-dimensional parameter spaces, such variance-based approaches can become computationally costly because the number of required simulations increases rapidly with the number of parameters (Saltelli et al., 1999; Marino et al., 2008). This motivates the use of efficient sampling strategies for ensemble-based uncertainty quantification, especially when comparing several different model complexity versions under identical parameter perturbations.

A sensitivity analysis based framework was previously developed to simplify marine BGC models while preserving key mechanisms, model interpretability, and acceptable fidelity to the full-complexity (FULL) version (Zhang et al., 2026). However, that study focused primarily on computational efficiency and on the ability of the simplified versions to reproduce the behaviour of the FULL version. Building on this framework, the present study addresses a different question: whether the simplified versions also preserve patterns of parameter-induced uncertainty. We investigate this question using the Eco3M-

https://doi.org/10.5194/egusphere-2026-5134
Preprint. Discussion started: 8 September 2026

MED-V1b model, and the two simplified versions, MOD1 and MOD2, were derived from the FULL version. In this study, FULL, MOD1, and MOD2 are all run in the same one-dimensional vertical (1DV) configuration and are forced with an identical parameter ensemble generated from a Sobol low-discrepancy sequence (Sobol, 1967).

Using this design, we first characterise the magnitude and time–depth distribution of parameter-induced uncertainty in the FULL version. We then compare MOD1 and MOD2 with FULL to determine whether simplification preserves these uncertainty patterns, or instead shifts the ensemble median, changes the uncertainty spread, and modifies the distribution of key state variables, biogeochemical fluxes, and ecosystem indicators. Specifically, this study addresses three questions: (i) What are the magnitude and time–depth distribution of parameter-induced uncertainty in the FULL version? (ii) To what extent do MOD1 and MOD2 reproduce the ensemble distributions and uncertainty patterns of FULL? (iii) What are the implications for uncertainty propagation towards higher trophic levels?

The remainder of the paper is organised as follows: Section 2 presents the Eco3M-MED-V1b model, the generation of two simplified versions, the targeted state variables and ecosystem indicators, and the design of the parameter-induced uncertainty quantification experiment. Section 3 first characterises the parameter-induced uncertainty in the FULL version, and then compares the simplified versions with FULL in terms of ensemble medians, uncertainty spreads, and ecosystem indicators' distributions. Section 4 discusses the implications of these results for the evaluation and use of simplified marine biogeochemical models. Finally, Section 5 summarises the main conclusions and perspectives.

2 Material and Methods

2.1 Eco3M-MED-V1b model and its simplified versions

2.1.1 Description of Eco3M-MED-V1b model

The marine BGC model used in this study is Eco3M-MED-V1b in its 1DV configuration, which is implemented within the modular Eco3M platform (Baklouti et al., 2006). Eco3M-MED-V1b is a flexible-stoichiometry phytoplankton functional type (PFT) model. Its general structure is inherited from the Eco3M-MED version described by Baklouti et al. (2021), while the updates are described in **S1** of *Supplementary Material* of the present paper and more detailed in Baklouti et al. (under review). The model explicitly represents six plankton groups and includes 37 state variables distributed in seven compartments (Fig. 1): phytoplankton (PHY), heterotrophic bacteria (BAC), a micro/nano-zooplankton compartment (UZOO) combining nanoflagellates (HNF) and ciliates (CIL), mesozooplankton (MZOO), detritus (DET), dissolved organic matter (DOM), and inorganic nutrients (NUT). The NUT pool comprises nitrate (NO_3), ammonium (NH_4), and phosphate (PO_4), whereas DOM and DET represent organic matter. DET is further divided into small (DETS) and large (DETL) particles detritus, with distinct sinking velocities, enabling size-dependent export and remineralisation pathways. Major processes are represented mechanistically, including photosynthesis and photo-acclimation, nutrient and DOM uptake, grazing and associated excretion, mortality, particulate organic matter hydrolysis, nitrification, and remineralisation.

https://doi.org/10.5194/egusphere-2026-5134
Preprint. Discussion started: 8 September 2026

Furthermore, a distinctive feature of the model is that each PFT is described not only by biomass components (C, N, P, and chlorophyll (Chl)) but also by an explicit abundance (cells or individuals per unit volume). This allows the diagnostic computation of intracellular cell quotas (Q_X) and intracellular elemental ratios (Q_{XY}), which are subsequently used to regulate key biogeochemical rates through quota- and ratio-dependent feedback functions.

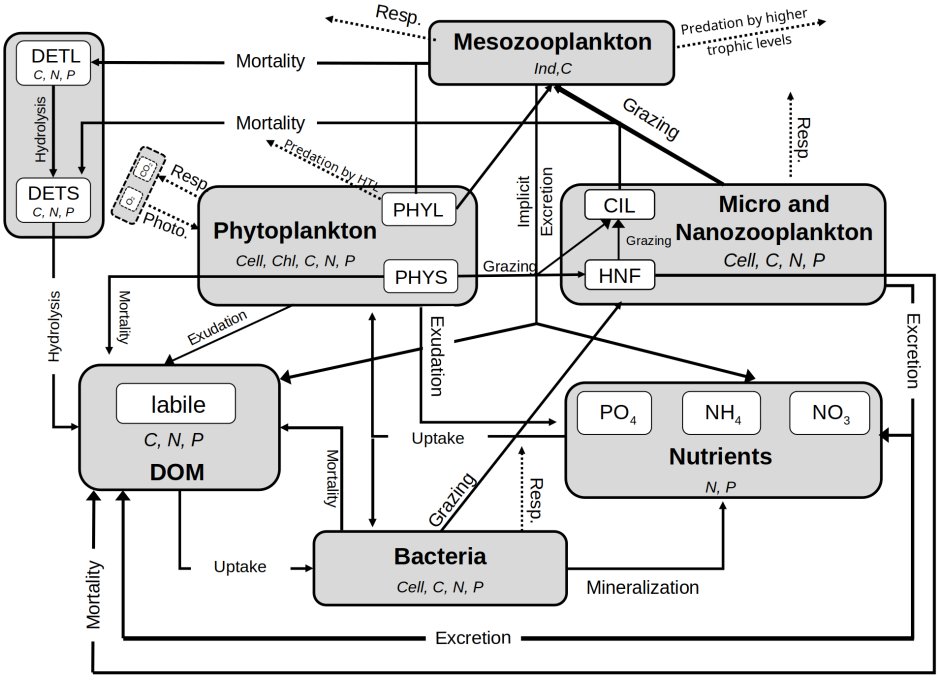

Figure 1. Conceptual representation of the Eco3M-MED-V1b model, adapted from Baklouti et al. (2021). Grey boxes denote the main biogeochemical compartments, while arrows indicate the direction of matter and energy flows between sub-compartments.

2.1.2 Eco3M-MED-V1b model simplification

We applied the semi-automated sensitivity-based simplification framework (Zhang et al., 2026) to the updated Eco3M-MED-V1b FULL version, and produced two simplified versions: MOD1 and MOD2. MOD1 was designed to preserve the fidelity of all the state variables, whereas MOD2 was designed to preserve the fidelity of selected marine ecosystem and biogeochemical indicators (Section 2.2). Relative to FULL, MOD1 reduced CPU computation time by 15%, whereas MOD2 reduced it by 23% in the 1DV model configuration (the reduction extends to 26% in 3D configuration). The main simplifications implemented in the two reduced versions are summarised in Table 1.

https://doi.org/10.5194/egusphere-2026-5134
Preprint. Discussion started: 8 September 2026

Table 1. Processes simplified or reduced in MOD1 and MOD2 relative to FULL. The check mark (✓) indicates that the corresponding process is fully removed, a cross (×) indicates that it is maintained as in FULL, and a circle (◯) indicates that it is only partially simplified.

	Reduced in		
Process	**MOD1**	**MOD2**	**Main changes due to simplification**
NH_4 and PO_4 uptake energetic costs	✓	✓	The additional carbon costs associated with NH_4 and PO_4 uptake are removed. As a result, nutrient uptake becomes less costly, leaving slightly more carbon available for PHY and BAC growth.
MZOO faecal-pellet routing	✓	✓	The faecal-pellet pathway is removed, which can reduce the transfer of carbon to DETL and weaken this export pathway.
O_2-related biological fluxes	◯	◯	In MOD1, the O_2 flux no longer includes zooplankton respiration, PHYS photosynthetic production, or the O_2 costs linked to PHY growth and nutrient uptake. Only BAC respiration, nitrification-related O_2 consumption, and PHYL photosynthetic production are retained. In MOD2, nitrification-related O_2 consumption is also removed.
NO_3 uptake energetic cost	×	✓	The additional carbon cost of NO_3 uptake is removed in MOD2, which can slightly favour nitrate uptake and leave slightly more carbon available for PHY and BAC growth.
Nitrification	×	✓	The explicit conversion of NH_4 to NO_3 is removed, together with the associated O_2 consumption.
Representation of inorganic nitrogen	×	✓	NO_3 and NH_4 are merged into one dissolved inorganic nitrogen (DIN) pool, resulting in a more compact representation of the nitrogen cycle.

2.2 Marine ecosystem indicators and state variables

To quantify model parameter-induced uncertainty and assess the effects of model simplification, we analysed a set of marine ecosystem and biogeochemical indicators, flux and state variables. These outputs were selected to represent the major dimensions of the marine ecosystem, including nutrient distributions, oxygen dynamics, trophic structure, autotrophic and heterotrophic production, planktonic biomass, and carbon export.

Two categories of model outputs were considered (see Table 2). The first category comprised seven state variables together with DETL carbon export flux (denoted as I_{var}), which was included as a key diagnostic of the biological carbon pump. These outputs were used to characterize the temporal and vertical distribution of the ecosystem and to identify where and when uncertainty patterns emerged. The second category comprised 15 ecosystem indicators (denoted by I_{ind}), which were used to synthesise annual or seasonal ecosystem properties. These indicators were largely consistent with those selected by Zhang et al. (2026), with the addition of three indicators: the summer mean nitracline depth (z_{nit}), the summer mean phosphacline depth (z_{pho}), and the annual mean surface Chl concentration ($\mathrm{Chl}_{surf}^{mean}$).

In addition to the model-to-model comparison, NO_3, PO_4, and Chl observation profiles from the DYFAMED station (43°N, 7.9°E) were used to provide an observational consistency check for the FULL ensemble simulations. The purpose of this comparison was to assess whether the simulated 5th–95th percentile envelope covered the main range of representative observed profiles. The observational data were obtained from the long-term DYFAMED time series maintained within the French

https://doi.org/10.5194/egusphere-2026-5134
Preprint. Discussion started: 8 September 2026

Table 2. Marine ecosystem and biogeochemical state variables and indicators considered in the model uncertainty quantification.

Symbol	Unit	Description
$I_{\mathrm{var}}(z,t)$: State variables and carbon export flux		
DIN	μmol L^{-1}	Dissolved inorganic nitrogen concentration ($NO_3 + NH_4$)
PO_4	μmol L^{-1}	Phosphate concentration
O_2	μmol L^{-1}	Dissolved oxygen concentration
BPHY	mg C m^{-3}	Phytoplankton biomass
BBAC	mg C m^{-3}	Bacterial biomass
BUZOO	mg C m^{-3}	Nano- and microzooplankton biomass
BMZOO	mg C m^{-3}	Mesozooplankton biomass
EXP_C	g C m^{-3} d^{-1}	Large detrital carbon (DETL) export flux
I_{ind}: Ecosystem indicators		
z_{nit}	m	Summer mean nitracline depth
z_{pho}	m	Summer mean phosphacline depth
z_{DCM}	m	Summer mean depth of the deep Chl maximum (DCM)
DCM_{con}	μg Chl L^{-1}	Summer mean Chl concentration at the DCM
Chl^{mean}_{surf}	μg Chl L^{-1}	Annual mean surface Chl concentration
GPP	g C m^{-2} yr^{-1}	Annual depth-integrated gross primary production
GSP	g C m^{-2} yr^{-1}	Annual depth-integrated gross secondary production
GBP	g C m^{-2} yr^{-1}	Annual depth-integrated gross bacterial production
$O2^{mean}_{0-600}$	μmol L^{-1}	Annual mean oxygen concentration in the 0–600 m layer
$BZOO^{mean}_{0-600}$	mg C m^{-3}	Annual mean total zooplankton biomass (MZOO + CIL + HNF) in the 0–600 m layer
$BMZOO^{mean}_{0-600}$	mg C m^{-3}	Annual mean mesozooplankton biomass in the 0–600 m layer
QC_{MZOO}	mg C ind^{-1}	Annual mean carbon quota, used as a proxy for relative MZOO individual size
$EXP_{C,100}$	g C m^{-2} yr^{-1}	Annual integrated DETL export at 100 m
$EXP_{C,1500}$	g C m^{-2} yr^{-1}	Annual integrated DETL export at 1500 m
TTE	–	Trophic transfer efficiency, defined as $GSP/(GPP + GBP)$

Note: z_{nit} and z_{pho} were defined as the depths of the first sustained reappearance of NO_3 and PO_4 in the vertical profiles, using thresholds of 0.5 μmol L^{-1} for NO_3 and 0.03 μmol L^{-1} for PO_4, following Marañón et al. (2021) for the Mediterranean Sea.

MOOSE program (Coppola et al., 2023). To remain consistent with the physical forcing used in the simulations, only observations from the year 2003 were used in the comparison.

2.3 Design of the parameter-induced uncertainty quantification experiment

The parameter-induced UQ was performed for the FULL version of Eco3M-MED-V1b and two simplified versions, first to quantify the parameter-induced output uncertainty associated with the shared parameters among the three model versions, and then to assess how model simplification affects this uncertainty. To ensure a consistent comparison, all simulations of FULL, MOD1, and MOD2 were conducted in a 1DV model configuration at the DYFAMED station, and used the same external

https://doi.org/10.5194/egusphere-2026-5134
Preprint. Discussion started: 8 September 2026

physical forcing, initial and boundary conditions, and numerical settings, only independent parameters shared by the three versions were perturbed (Table 3). Each simulation consisted of two consecutive runs using the same annual forcing, the first year was used as a spin-up period, and only the second year was retained for the analysis.

2.3.1 Selection of uncertain parameters and uncertainty ranges

The UQ experiment was applied to a subset of parameters shared by the three model versions ($n = 30$). For each parameter p_i, a reference value (p_i^{ref}) was defined and used in the reference simulation (denoted by $\hat{m}$). The 30 shared parameters were classified into three groups according to prior confidence levels and expert knowledge: well-constrained (WC, $n = 11$), moderately-constrained (MC, $n = 15$), and uncertain (UC, $n = 4$) as defined in Zhang et al. (2026). A group-specific uncertainty factor $f_i \in \{0.20, 0.40, 0.80\}$ was assigned to each group, and this factor was used to define a symmetric uncertainty interval ($\Phi_{i,\mathrm{unc}}$) around the reference value (*cf.* Eq. 1).

$$\Phi_{i,\mathrm{unc}} = \left(p_i^{\mathrm{ref}} - f_i p_i^{\mathrm{ref}},\ p_i^{\mathrm{ref}} + f_i p_i^{\mathrm{ref}}\right) \tag{1}$$

The final effective interval ($\Phi_{i,\mathrm{eff}}$) used for UQ is constructed based on the group-specific uncertainty interval, available literature information, and expert judgement, following the rules described in Appendix A. This approach preserves the *a priori* uncertainty magnitude while incorporating available literature information and expert judgement. Table 3 summarises the parameter symbols, reference values, groups, and descriptions. As a concrete example, the turnover time for small detritus hydrolysis (τ_{DETS}^{hyd}), was varied from 2.1 to 18.9 days around a reference value of 10.5 days. This range spans faster to slower remineralisation regimes, affecting both the recycling of DETS into dissolved pools and its potential contribution to downward carbon transfer. The literature references for each parameter are provided in Appendix B.

For parameters with literature-based bounds, samples were drawn from bounded Beta distributions over $\Phi_{i,\mathrm{eff}}$, with the reference value (p_i^{ref}) used as the distribution mode. The Beta distributions are defined using the mode–concentration parametrisation (κ_i), which follows the width-based rule described in Appendix A4. By contrast, parameters for which no literature-based bounds are available, are sampled from a uniform distribution defined over $\Phi_{i,\mathrm{unc}}$.

2.3.2 Generation of parameter ensemble using Sobol sequence

The parameter ensemble used for the parameter-induced uncertainty quantification was generated with a Sobol low-discrepancy sequence (Sobol, 1967; Bratley and Fox, 1988). Although Sobol sequences are often associated with Sobol sensitivity analysis, here they were used solely to generate quasi-random samples for uncertainty quantification, and Sobol sensitivity indices were not estimated. Compared with pseudo-random sampling, low-discrepancy sequences generally provide a more uniform coverage of the parameter space for a given computational budget, which can improve the efficiency of ensemble-based uncertainty analyses (Saltelli et al., 1999). The deterministic and extensible nature of the Sobol sequence also makes the sampling design reproducible and allows the ensemble to be progressively extended without redefining the initial sampling scheme. This prop-

https://doi.org/10.5194/egusphere-2026-5134
Preprint. Discussion started: 8 September 2026

Table 3. Descriptions of the parameters shared among the three model versions and used for UQ. More details are provided in Appendix B.

Parameter	Unit	p_i^{ref}	Group	Description
H_{BAC}	μm	0.5	WC	Semi-major axis of BAC ellipsoidal cell
H_{PHYS}	μm	0.5	WC	Semi-major axis of PHYS ellipsoidal cell
H_{PHYL}	μm	10.0	WC	Semi-major axis of PHYL ellipsoidal cell
V_{HNF}	μm^3	17.4	WC	Cell volume of HNF
V_{CIL}	μm^3	$1.64\ 10^4$	WC	Cell volume of CIL
r_{QC}	–	3.0	WC	Carbon quota ratio
r_{CNmin}	mol C (mol N)$^{-1}$	4.0	WC	Minimum C:N quota ratio
CN_{max}	–	22.0	WC	Maximum C:N quota ratio
CP_{max}	mol C (mol P)$^{-1}$	300.0	WC	Maximum C:P quota ratio
r_{uLDOC}	–	0.1	WC	Energetic cost of labile dissolved organic carbon (LDOC) assimilation
μ_{MZOO}	s^{-1}	$7.0\ 10^{-7}$	WC	Maximum specific growth rate of MZOO
$Q_{C_{MZOO}}^{\mathrm{mean}}$	mol C ind^{-1}	$5.0\ 10^{-7}$	MC	Mean intracellular carbon quota of MZOO
$Q_{C_{BAC}}^{\mathrm{mean}}$	mol C cell^{-1}	$1.67\ 10^{-15}$	MC	Mean intracellular carbon quota of BAC
A_{CIL}	cell L^{-1}	$3.0\ 10^3$	MC	Typical abundance of CIL
A_{PHYL}	cell L^{-1}	$2.0\ 10^5$	MC	Typical abundance of PHYL
A_{HNF}	cell L^{-1}	$1.0\ 10^6$	MC	Typical abundance of HNF
A_{PHYS}	cell L^{-1}	$5.0\ 10^7$	MC	Typical abundance of PHYS
A_{BAC}	cell L^{-1}	$3.0\ 10^8$	MC	Typical abundance of BAC
$\theta_{C,PHYL}^{max}$	g Chl mol C^{-1}	1.2	MC	Maximum Chl-to-carbon ratio of PHYL
St_{BAC}	–	0.0125	MC	Fraction of BAC surface covered by uptake sites
α_{PHYS}^{B}	mol C m^2 gChl^{-1} J^{-1}	$1.72\ 10^{-6}$	MC	Initial light-limited slope for PHYS
α_{PHYL}^{B}	mol C m^2 gChl^{-1} J^{-1}	$1.84\ 10^{-6}$	MC	Initial light-limited slope for PHYL
r_{gHET}	–	0.3	MC	Energetic cost of heterotrophic growth
r_{phy}	–	2.0	MC	Major/minor axis ratio of phytoplankton cells
r_{bac}	–	5.0	MC	Major/minor axis ratio of bacterial cells
r_m^{PFT}	–	25.0	MC	Ratio between maximum growth rate and mortality rate
τ_{hyd}^{DETS}	day	10.5	UC	Turnover time for DETS hydrolysis
τ_{hyd}^{DETL}	day	4.5	UC	Turnover time for DETL hydrolysis to DETS
k_{mq}^{MZOO}	ind^{-1} s^{-1}	$1.4\ 10^{-7}$	UC	Quadratic mortality coefficient of MZOO
k_{mq}^{PHYL}	cell^{-1} s^{-1}	$3.0\ 10^{-12}$	UC	Quadratic mortality coefficient of PHYL

https://doi.org/10.5194/egusphere-2026-5134
Preprint. Discussion started: 8 September 2026

erty is useful when simulations are performed in successive batches or when the stability of uncertainty estimates is assessed with increasing ensemble size.

Based on the parameter distributions and effective bounds defined above, $N = 2^9 = 512$ parameter sets were generated using a Sobol low-discrepancy sequence. Each Sobol point was transformed into a parameter vector according to the prescribed parameter distributions and effective uncertainty bounds (see Appendix A4). The same ensemble of parameter vectors was applied to FULL, MOD1, and MOD2, enabling one-to-one comparisons (see **S4** in *Supplementary material*) under identical parameter perturbations and thereby reducing sampling-induced differences among model versions. The choice of $N = 512$ was based on an empirical convergence assessment (see **S3** in *Supplementary material*) using successive nested subsets of the same extensible Sobol sequence ($N = 16, 32, 64, 128, 256, 512$), and $N = 512$ was retained as a compromise between convergence stability and computational cost. Since each parameter set was applied to all three model versions, $N = 512$ required 1536 simulations in total.

2.3.3 Uncertainty diagnostics and statistical metrics

Following previous ensemble-based uncertainty quantification studies (e.g. Murphy et al., 2004; Smith et al., 2009), parameter-induced uncertainty was summarised using quantile-based statistics of the model ensemble. For each model version and each output, the ensemble distribution was obtained from the set of parameter samples, and its quantile of order α was denoted by q_α. In addition, $\hat{m}$ denotes the model output obtained with the reference parameter set p^{ref} (*cf.* Table 3).

The ensemble median was defined as:

$$\widetilde{m} = q_{0.50} \tag{2}$$

The uncertainty spread was defined as the width of the central 90% interval:

$$\Delta = q_{0.95} - q_{0.05} \tag{3}$$

where $q_{0.05}$ and $q_{0.95}$ are the 5th and 95th percentiles, respectively.

To assess how uncertainties are modified by the simplification process, these statistics were compared between each simplified version ($\mathrm{S} \in \{\mathrm{MOD1}, \mathrm{MOD2}\}$) and the FULL version. The following difference based metrics were used:

$$\begin{aligned} \phi(\widetilde{m}^S) &= \widetilde{m}^S - \widetilde{m}^{FULL}, \\ \phi(\Delta^S) &= \Delta^S - \Delta^{FULL}, \\ \phi(\log_{10}\Delta^S) &= \log_{10}(\Delta^S) - \log_{10}(\Delta^{FULL}). \end{aligned} \tag{4}$$

Here, $\phi(\widetilde{m}^S)$ describes the shift in the ensemble median caused by model simplification. $\phi(\Delta^S)$ quantifies the absolute change in uncertainty spread relative to FULL. Finally, $\phi(\log \Delta^S)$ provides a dimensionless measure of the relative change in uncertainty spread, and is therefore useful for comparing uncertainty changes in outputs with different units.

https://doi.org/10.5194/egusphere-2026-5134
Preprint. Discussion started: 8 September 2026

2.4 Distributional comparison using the Kolmogorov–Smirnov statistic

To identify which ecosystem indicators were most affected by model simplification, we compared the ensemble distribution of each simplified version with that of the FULL version using the Kolmogorov-Smirnov (K–S) statistic (Massey, 1951). This statistic compares the entire empirical cumulative distribution and is therefore well-suited for detecting changes in distributional behaviour, including shifts in median, changes in spread, or modifications of distribution shape. For each indicator and simplified version S, the K–S statistic D was calculated as

$$D = \sup_x |F_{\mathrm{FULL}}(x) - F_{\mathrm{S}}(x)|, \tag{5}$$

where $F_{\mathrm{FULL}}(x)$ and $F_{\mathrm{S}}(x)$ are the empirical cumulative distribution functions of the FULL and simplified version ensembles, respectively. Larger values of D (ranging from 0 to 1) indicate stronger differences between the two ensemble distributions. In this study, the statistic D was used to quantify the magnitude of the distributional difference. $\phi(\widetilde{m}^S)$ and $\phi(\Delta^S)$ were then used to determine whether simplification mainly shifted the median or modified the parameter-induced uncertainty spread.

3 Results

In the results section, we first characterise parameter-induced uncertainty in FULL and compare the FULL ensemble with observations. We then examine the effects of simplification on state variables and carbon export, and finally evaluate the changes in ecosystem indicators.

3.1 Parameter-induced uncertainty patterns in FULL version

3.1.1 Time–depth distribution of parameter-induced uncertainty

We first analysed the time–depth distribution of the main statistical metrics for the FULL version to characterise the baseline pattern of parameter-induced uncertainty (Fig. 2). As the ensemble median does not represent the output of any single model simulation (it is derived at each time and depth from the median value of all ensemble simulations), we provide in **S2** of the *Supplementary Material* the distribution of the reference simulation and its difference from the ensemble median. In addition, the locations and values of the maximum uncertainty spreads are summarised in Table 4

Table 4. Locations and values of the maximum Δ^{FULL} for the state variables and carbon export flux in the FULL version. Depths correspond to the model vertical z-coordinate levels. Values in brackets indicate the corresponding maximum Δ^{FULL}.

DIN	PO_4	O_2	BPHY	BBAC	BUZOO	BMZOO	EXP_C
Sep, 66.1 m	Oct, 78.2 m	Sep, 66.1 m	Apr, 0.5 m	May, 11.4 m	Jun, 40.5 m	May, 18.5 m	Apr, 92.7 m
[5.45]	[0.24]	[28.91]	[62.80]	[7.19]	[77.17]	[48.87]	[0.18]

Note: Units are μmol L^{-1} for DIN, PO_4, and O_2; mg C m^{-3} for BPHY, BBAC, BUZOO, and BMZOO; and g C m^{-2} d^{-1} for EXP_C.

https://doi.org/10.5194/egusphere-2026-5134
Preprint. Discussion started: 8 September 2026

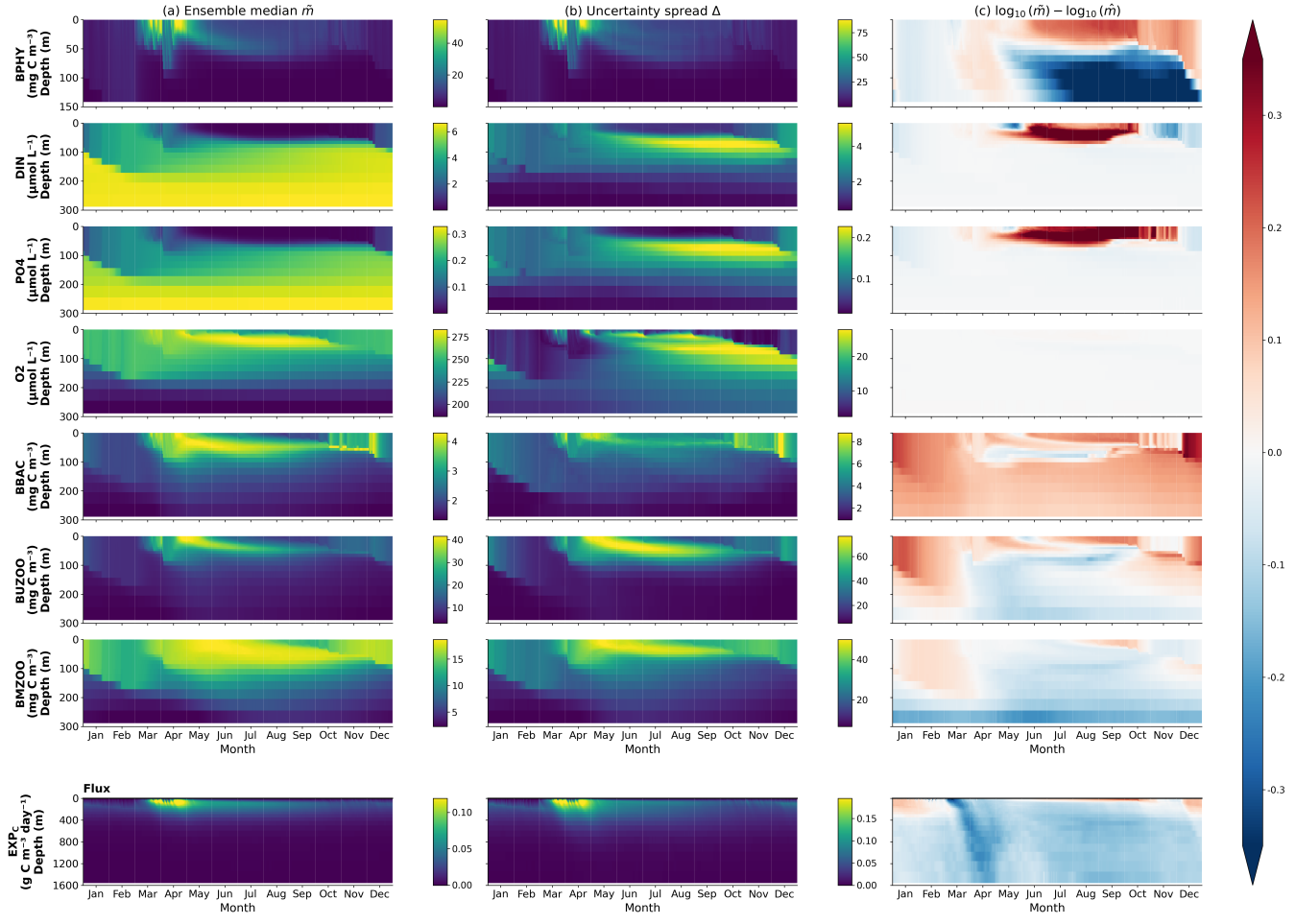

Figure 2. Time–depth distribution of the statistical metrics for the FULL version. The left column (a) shows the ensemble median $\tilde{m}^{FULL}$, the middle column (b) shows the ensemble uncertainty spread Δ^{FULL}, and the right column (c) shows the logarithmic ratio $\log_{10}(\tilde{m}^{FULL}/\hat{m}^{FULL})$ between the FULL ensemble median and the reference simulation. For interpretation, values of $+0.3$ (dark red) indicate that the ensemble median is approximately twice the reference value, while values of -0.3 (dark blue) indicate that it is approximately half the reference value. The displayed depth range differs among state variables and flux: BPHY is shown in the upper 150 m, $\mathrm{EXP_C}$ down to 1600 m, and the other variables in the upper 300 m, as values in deeper layers were nearly stable and showed no marked variation.

Specifically, BPHY showed high median values in the euphotic layer and near the DCM, with the largest uncertainty occurring near the surface during the spring bloom. DIN and PO_4 showed lower median concentrations in the upper 0–150 m than in deeper layers, especially during the stratified summer–autumn period, while concentrations increased with depth. Their largest uncertainty spreads occurred near the upper nutricline (Table 4). A similar vertical pattern was observed for O_2, although its uncertainty spread remained small relative to the median concentration, which generally ranged from 200 to 280 μmol L^{-1}.

https://doi.org/10.5194/egusphere-2026-5134
Preprint. Discussion started: 8 September 2026

The heterotrophic compartments also showed marked uncertainty during the productive season. Among them, BMZOO exhibited a deeper vertical extension of uncertainty than the other biological variables. For EXP_C, the response was more clearly concentrated around the spring bloom than for the other biological variables (except BPHY). Both the ensemble median and the uncertainty spread increased during the productive period, mainly in the upper 0–200 m, and then weakened after the bloom (Table 4).

The logarithmic ratio (Fig. 2(c)) indicated that the ensemble median generally remained close to the reference simulation. Deviations were weak for DIN and PO_4 and were mainly confined to the upper layer during the stratified period, while O_2 showed almost no deviation. In contrast, BPHY showed positive deviations in the near-surface layer and negative deviations below during the summer–autumn period (due to the very low BPHY concentrations). Zooplankton compartments displayed clearer vertical patterns, with positive deviations generally occurring in the upper layer and negative deviations below. For EXP_C, negative deviations appeared after the spring bloom and progressively extended downward.

In conclusion, parameter-induced uncertainty in the FULL version was not uniformly distributed. It was mainly concentrated during the spring bloom, near the upper nutricline, and within the euphotic layer, depending on the variable considered. In contrast, the ensemble median remained generally close to the reference simulation.

3.1.2 Comparison between observational and ensemble uncertainty envelopes

The FULL ensemble was further compared with observational profiles of NO_3, PO_4, and Chl at the DYFAMED station to evaluate whether the parameter-induced uncertainty range was consistent with the observed seasonal vertical structure (Fig. 3).

For nutrients, the FULL version reproduced the main seasonal contrast between nutrient-depleted surface waters and nutrient-rich deeper waters. The observed NO_3 and PO_4 profiles were generally close to the FULL reference simulation and ensemble median in spring. In summer and autumn, the model also represented the development and re-establishment of vertical nutrient gradients, although local differences remained near the nutricline and in the upper to intermediate layers. For Chl, the FULL version captured the main seasonal evolution of the vertical distribution. Observations were generally within or close to the ensemble envelope, especially in winter, while the ensemble spread was larger near the DCM.

For each seasonal profile, the coverage rate was defined as the fraction of observed depth levels falling within the 5th–95th percentile envelope of the FULL ensemble. For NO_3, the coverage rates were 53.8%, 60.0%, 30.0%, 75.0% in winter, spring, summer, autumn, respectively. The corresponding values were 61.5%, 60.0%, 44.4%, 77.8% for PO_4, and 100.0%, 74.3%, 87.8%, 63.5% for Chl. In general, the coverage was higher for Chl than for nutrients, whereas the lowest values occurred for nutrient profiles with sharp vertical gradients. These lower coverage values were mainly associated with the nutricline and the DCM position, where short-time or depth mismatches between observations and simulations can lead to large local differences.

These results also highlight an advantage of ensemble-based uncertainty quantification: the uncertainty envelope provides a more informative basis for comparison with observations than a single reference simulation.

https://doi.org/10.5194/egusphere-2026-5134
Preprint. Discussion started: 8 September 2026

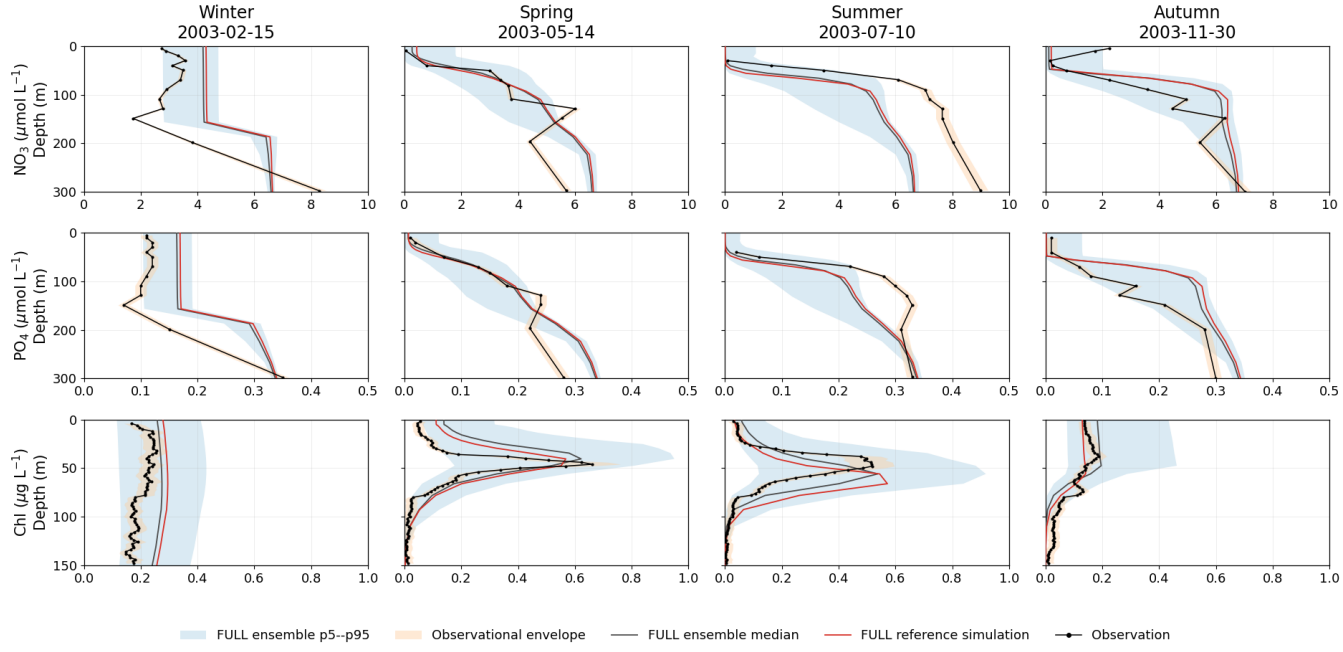

Figure 3. Seasonal vertical profiles of NO_3, PO_4, and Chl concentration at the DYFAMED station in 2003. Columns correspond to representative winter, spring, summer, and autumn observation dates, and rows correspond to the three observed variables. The blue shading indicates the uncertainty envelope of the FULL version ensemble, defined by the 5th and 95th percentiles. The grey line denotes the FULL ensemble median, and the red line denotes the reference simulation ($\hat{m}^{\mathrm{FULL}}$). The black line with markers shows the observation profile. The orange shading indicates the observational uncertainty envelope around the selected profile, defined at each depth as $\pm\max(0.01\ \mu\mathrm{mol\ L^{-1}}, 3\%)$ for NO_3 and PO_4, and as $\pm\max(0.02\ \mu\mathrm{g\ L^{-1}}, 15\%)$ for Chl.

3.2 State-variable responses to model simplification

3.2.1 Ensemble median differences

To assess how model simplification affects the spatio-temporal distribution of parameter-induced uncertainty, we compared the time–depth distributions of ensemble median differences between MOD1, MOD2, and FULL.

As shown in Fig. 4, the differences were generally stronger in MOD2. For BPHY, MOD1 was mostly lower than FULL in the upper layer from late spring to autumn. In MOD2, the response was stronger, with positive differences during the spring bloom and negative differences in the upper layer during summer and autumn. Below about 50 m, MOD2 also showed clearer positive differences than MOD1. For DIN and PO_4, both simplified versions produced lower ensemble median concentrations than FULL in the upper layer, especially outside the summer–autumn stratified period, while weak positive differences appeared below this layer. For O_2, the simplified models generally showed higher concentrations than FULL, except in the upper layer during summer and autumn, and the positive differences below the upper layer were much stronger in MOD2.

https://doi.org/10.5194/egusphere-2026-5134
Preprint. Discussion started: 8 September 2026

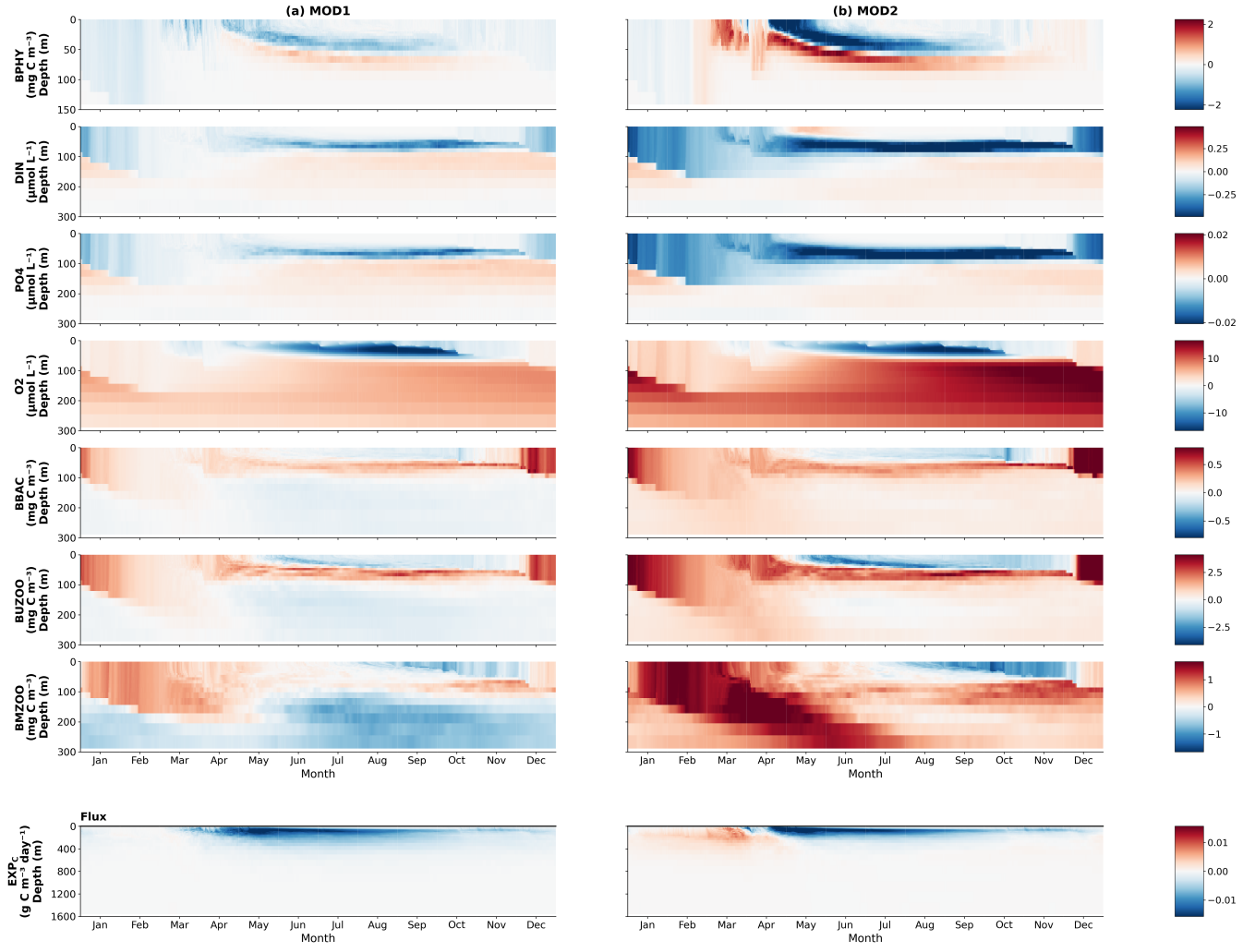

Figure 4. Time–depth distribution of ensemble-median differences ($\phi(\widetilde{m})$) between the simplified and FULL versions for the state variables and carbon export flux. The left (a) and right (b) columns show MOD1 and MOD2, respectively.

250 For the heterotrophic compartments, BBAC, BUZOO, and BMZOO generally showed positive differences in the upper water column during winter and spring, but weak negative differences during summer and autumn. At the deeper layer (>150 m), MOD1 tended to be lower than FULL, whereas MOD2 was mostly higher, especially for BMZOO below 200 m. Finally, both simplified versions showed mainly negative differences in $\mathrm{EXP_C}$ after the spring bloom, but MOD2 also presented a positive difference in early spring.

https://doi.org/10.5194/egusphere-2026-5134
Preprint. Discussion started: 8 September 2026

3.2.2 Distribution of uncertainty spread differences

We used logarithmic differences to express relative uncertainty differences between the simplified and FULL versions, as shown in Figure 5. In this logarithmic scale, values around ± 0.1 indicate moderate changes in uncertainty spread, while values close to ± 1 indicate changes of about one order of magnitude. The different ranges should therefore be interpreted as relative changes, rather than absolute differences.

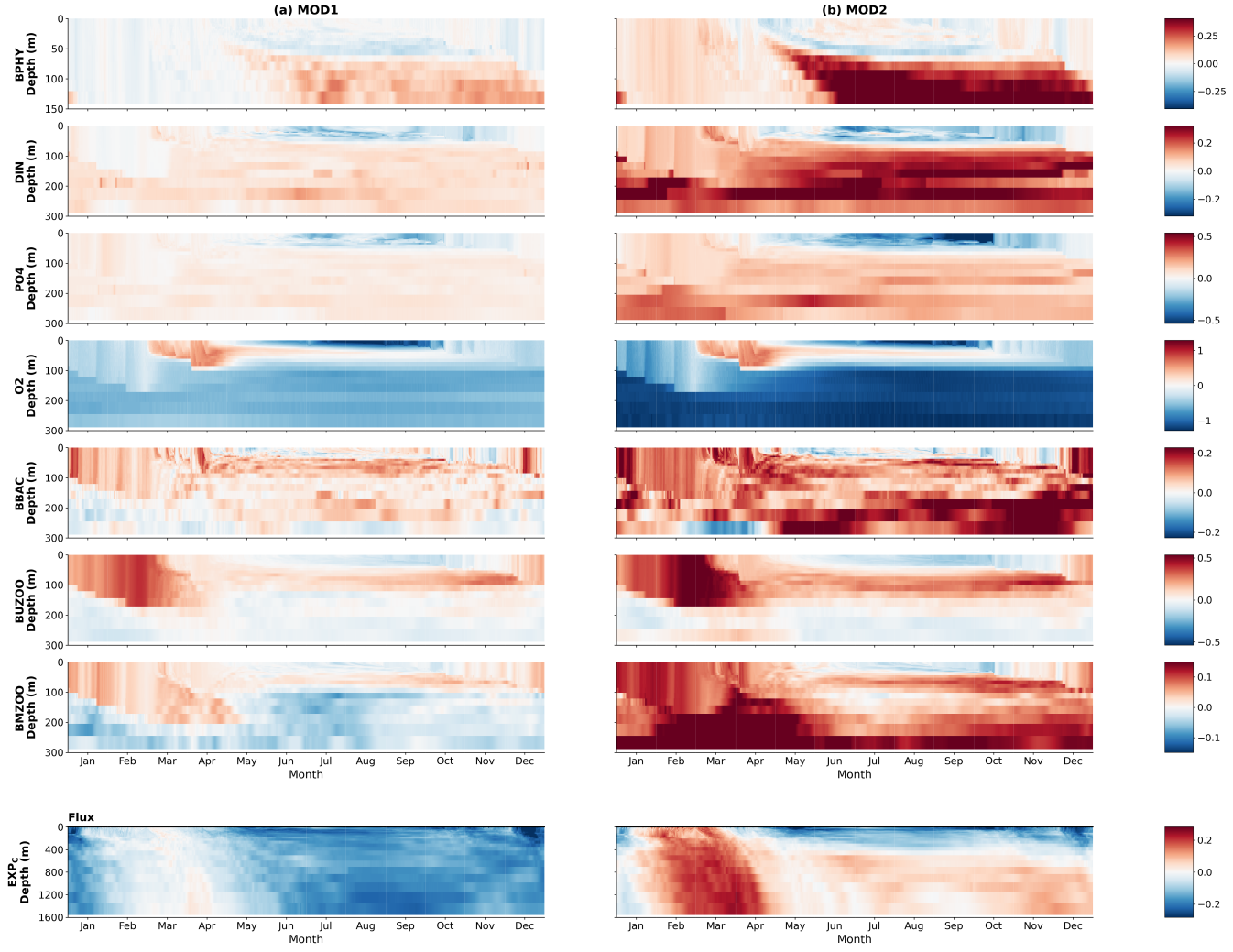

Figure 5. Time–depth distribution of the logarithmic differences in uncertainty spread ($\phi(\log_{10}\Delta^S)$) between the simplified versions and FULL for state variables and carbon export flux. The left (a) and right (b) columns correspond to MOD1 and MOD2, respectively. Positive values (red) indicate a larger uncertainty spread in the simplified version than in FULL, whereas negative values (blue) indicate a reduction in uncertainty spread.

https://doi.org/10.5194/egusphere-2026-5134
Preprint. Discussion started: 8 September 2026

For BPHY, MOD1 induced moderate changes, with uncertainty reduction mainly occurring in the upper layer during the stratified period and weak positive differences below. In contrast, MOD2 produced a clear uncertainty inflation below the upper layer after spring. For DIN and PO_4, the changes in MOD1 remained limited. In the upper layer, weak uncertainty inflation was observed during winter and spring, whereas uncertainty was reduced during the summer–autumn stratified period. Below the upper layer, a weak positive signal was generally present. In MOD2, the increase in nutrient uncertainty was more pronounced below the upper layer, particularly below 150 m. For O_2, both simplified versions generally reduced uncertainty relative to FULL, with a stronger reduction in MOD2, but local positive differences observed in the upper layer during spring. This reduction was particularly pronounced at depth, where O_2 variability is less directly influenced by air–sea exchange.

For the heterotrophic compartments, MOD2 generally produced larger uncertainty inflations than MOD1, particularly evident for BBAC and BUZOO, where enhanced uncertainty appeared in the upper and subsurface layers. For BMZOO, the positive differences extended deeper in the water column in MOD2 than in MOD1.

The response of $\mathrm{EXP_C}$ was the most contrasted between the two simplified versions. Since both simplified versions include the removal of the MZOO faecal-pellet pathway (Table 1), changes in $\mathrm{EXP_C}$ may partly reflect modifications in the routing of grazed carbon towards sinking DETL. In MOD1, the uncertainty spread was generally reduced over most of the water column, except during the bloom period, where weak positive differences appeared. In MOD2, uncertainty increased markedly from late winter to early spring and extended downward, whereas uncertainty reductions were mainly confined to the upper layer during the stratified period. Below the upper layer, MOD2 mainly showed uncertainty increasing.

These results show that simplification did not systematically increase the uncertainty spread. Both uncertainty increasing and uncertainty reduction were observed, depending on the variable, depth, and period considered. Although MOD2 generally produced stronger changes than MOD1, these changes were not always in the same direction, rather than simply increasing the uncertainty spread.

3.2.3 Quantification of uncertainty spread differences

Since Section 3.2.2 mainly describes relative changes in uncertainty spread through $\phi(\log_{10}\Delta)$, we further analysed the extrema of the uncertainty spread differences on the original scale ($\phi(\Delta)$) and identified their corresponding time–depth locations.

Among the 32 extrema of $\phi(\Delta)$ reported in Table 5, 29 occurred within the upper 150 m, and all negative extrema were located within this depth range. Only three positive extrema were found below 150 m, corresponding to EXP_C in both MOD1 and MOD2, and BMZOO in MOD2. Although $\phi(\log_{10}\Delta)$ revealed some vertically extensive relative signals, especially in MOD2, the largest absolute changes in uncertainty spread were mainly concentrated in the upper water column.

The seasonal locations of the extrema differed among variables. For nutrients, the maxima of $\phi(\Delta)$ occurred in September in MOD1 and in December in MOD2, whereas the minima were mainly found during summer or early autumn. For O_2, positive extrema occurred near the surface in May, while the strongest negative extrema appeared later in the year. For biological variables, positive extrema were mostly located between spring and autumn, whereas negative extrema mainly occurred from April to September. Furthermore, MOD2 produced larger uncertainty spread changes than MOD1 for most variables, especially for BPHY, BUZOO, BMZOO, and EXP_C.

https://doi.org/10.5194/egusphere-2026-5134
Preprint. Discussion started: 8 September 2026

Table 5. Locations of the extrema in the uncertainty difference $\phi(\Delta)$ for the simplified versions relative to the FULL version. In each cell, the first line gives the month and depth, and the second line gives the corresponding value of $\phi(\Delta)$.

(a) Maxima of $\phi(\Delta^{S})$

Model	DIN	PO_4	O_2	BPHY	BBAC	BUZOO	BMZOO	EXP_C
MOD1	Sep, 78.2 m [+0.28]	Sep, 110.2 m [+0.01]	May, 29.5 m [+5.09]	Jun, 66.1 m [+0.85]	Aug, 47.5 m [+0.59]	Oct, 66.1 m [+7.65]	Nov, 66.1 m [+1.61]	Feb, 267.1 m [$+7.60 \times 10^{-3}$]
MOD2	Dec, 131.2 m [+1.46]	Dec, 131.2 m [+0.04]	May, 29.5 m [+5.32]	Jun, 66.1 m [+2.98]	Aug, 47.5 m [+0.98]	Aug, 78.2 m [+11.71]	Mar, 186.9 m [+3.41]	Mar, 156.5 m [+0.34]

(b) Minima of $\phi(\Delta^{S})$

Model	DIN	PO_4	O_2	BPHY	BBAC	BUZOO	BMZOO	EXP_C
MOD1	Sep, 47.5 m [−0.29]	Jul, 40.5 m [−0.01]	Aug, 18.5 m [−13.53]	Apr, 2.7 m [−1.94]	Jul, 18.5 m [−0.44]	Aug, 29.5 m [−5.91]	Jul, 110.2 m [−1.62]	May, 78.2 m [−0.62]
MOD2	Sep, 47.5 m [−0.42]	Aug, 47.5 m [−0.02]	Nov, 110.2 m [−17.25]	Apr, 0.5 m [−4.74]	Jul, 18.5 m [−0.40]	Sep, 34.5 m [−7.12]	Aug, 21.7 m [−2.39]	May, 40.5 m [−0.67]

Note: The units of $\phi(\Delta)$ are μmol L^{-1} for DIN, PO_4, and O_2; mg C m^{-3} for BPHY, BBAC, BUZOO, and BMZOO; and g C m^{-2} d^{-1} for EXP_C.

3.3 Ecosystem indicator responses to model simplification

Compared with the state variable analysis presented above, ecosystem indicators provide a more integrated view of model behaviour. We therefore use them to assess how model simplification affects ensemble distributions, median responses, and parameter-induced uncertainty spreads.

3.3.1 Ecosystem indicator uncertainty in the FULL version

Before comparing the simplified versions with the FULL version, we first examined the uncertainty distribution of the ecosystem indicators within the FULL ensemble. The frequency distributions show contrasted uncertainty patterns among indicators (Fig. 6). Most indicators display unimodal distributions, but the degree of spread and skewness differ among indicators.

Figure 6 shows that most ecosystem indicators in the FULL ensemble were centred around a dominant response, with the reference simulation generally close to the ensemble median. However, the width and shape of the distributions differed strongly among indicators. The vertical-structure indicators, z_{nit}, z_{pho}, and z_{DCM}, were broadly centred near the reference simulation and the ensemble median, but their uncertainty spreads remained substantial. Phytoplankton-related indicators also showed contrasting behaviour. $\mathrm{DCM_{con}}$ and $\mathrm{Chl}_{surf}^{mean}$ were generally unimodal but right-skewed, indicating that some parameter combinations produced substantially higher Chl values than the reference simulation.

The production and trophic indicators showed larger differences in distribution shape. The O_2 indicator was relatively tightly distributed compared with its median value. GPP remained relatively close to the reference and median values, whereas GBP showed a much broader and strongly right-skewed distribution. GSP and the zooplankton-related indicators also displayed marked spread and right-skewness, especially $\mathrm{BZOO}_{0-600}^{mean}$ and $\mathrm{BMZOO}_{0-600}^{mean}$.

Carbon export exhibited a clear contrast between shallow and deep export. $\mathrm{EXP}_{C,100}$ had a broad but relatively continuous distribution, with $\Delta^{FULL} = 27.3$ g C m^{-2} yr^{-1}. This spread was of the same order as the ensemble median, indicating that annual carbon export at 100 m was strongly affected by parameter-induced uncertainty. In contrast, $\mathrm{EXP}_{C,1500}$ was strongly right-skewed, with many ensemble members close to very low export values and a long tail towards higher values. Similar near-

https://doi.org/10.5194/egusphere-2026-5134
Preprint. Discussion started: 8 September 2026

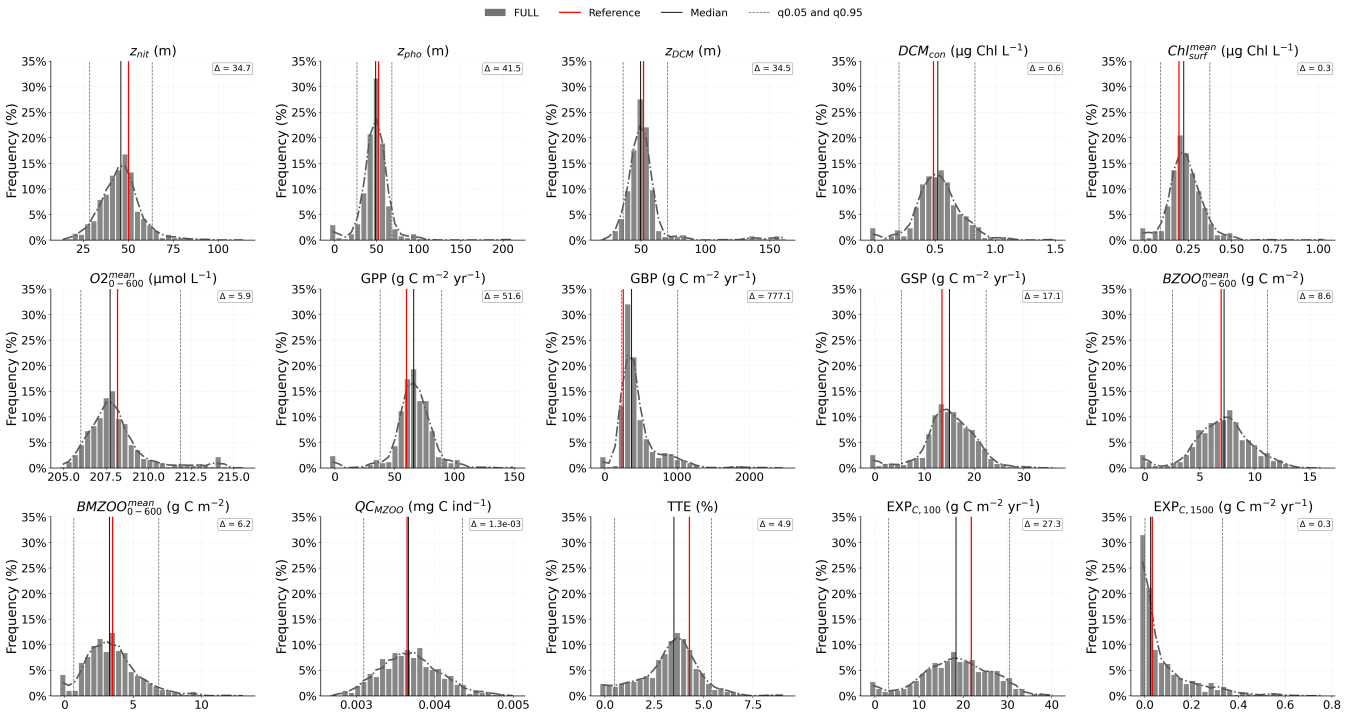

Figure 6. Frequency distributions of ecosystem indicators (I_{ind}) across the 512-member ensemble of FULL version. Grey histograms show the relative frequency distributions of ensemble values. The red vertical line indicates the reference simulation ($\hat{m}$), the solid black line denotes the ensemble median ($\widetilde{m}$), and the dashed grey lines mark the 5th and 95th percentiles ($q_{0.05}$ and $q_{0.95}$). The grey dash-dotted curve shows the smoothed distribution. The value reported in the upper-right corner of each panel corresponds to the ensemble uncertainty spread, defined as $\Delta^{FULL} = q_{0.95} - q_{0.05}$.

zero responses were also visible for some biological indicators, such as $\mathrm{DCM_{con}}$, GBP, and zooplankton biomass indicators. This indicates that some parameter combinations can push the model towards low-activity biological states (see **S4** and **S5** in *Supplementary Material*), while others generate much stronger trophic or export responses.

3.3.2 Effects of simplification on ecosystem indicators

To assess how simplification modified the ensemble behaviour of ecosystem indicators, the K–S statistic D (Table 6a; Section 2.4) was used to quantify differences between the ensemble distributions of each simplified version and FULL. Relative differences in the ensemble median (Table 6b) and uncertainty spread (Table 6c) were then used to distinguish changes in the median from changes in parameter-induced uncertainty. Moreover, six representative indicators showing contrasting responses to model simplification are presented in Figure 7.

For the vertical-structure indicators, the median of z_{pho} and z_{DCM} increased in both MOD1 and MOD2. Changes in uncertainty spread were limited in MOD1, whereas MOD2 slightly increased the spread of both indicators, and with stronger

https://doi.org/10.5194/egusphere-2026-5134
Preprint. Discussion started: 8 September 2026

Table 6. Distributional fidelity metrics of the simplified versions ($S \in \{MOD1, MOD2\}$) relative to FULL. The table reports the K–S statistic D, the relative difference in ensemble median ($(\widetilde{m}^{S} - \widetilde{m}^{FULL})/\widetilde{m}^{FULL}$), and the relative difference in uncertainty spread ($(\Delta^{S} - \Delta^{FULL})/\Delta^{FULL}$).

Indicator	(a) K–S statistic D value		(b) Relative median difference (%)		(c) Relative spread difference (%)	
	MOD1	MOD2	MOD1	MOD2	MOD1	MOD2
z_{nit}	0.11	–	+3.9	–	−2.9	–
z_{pho}	0.09	0.20	+3.4	+8.5	−0.9	+6.0
z_{DCM}	0.09	0.15	+3.1	+4.9	−0.9	+5.2
DCM_{con}	0.06	0.10	−4.3	−7.3	−3.1	−8.3
Chl^{mean}_{surf}	0.06	0.09	−2.4	−4.5	−2.4	−2.9
$O_{2\,0\text{–}600}^{mean}$	0.68	0.94	+0.9	+2.7	−43.0	−57.0
GPP	0.06	0.11	−2.2	−3.8	−2.4	−1.4
GBP	0.11	0.23	+6.2	+17.3	−0.6	+7.6
GSP	0.02	0.19	+0.3	+12.8	−0.1	+13.5
$BZOO^{mean}_{0\text{–}600}$	0.03	0.16	−1.4	+10.3	−1.2	+10.2
$BMZOO^{mean}_{0\text{–}600}$	0.04	0.09	−4.1	+6.2	−3.3	+10.0
QC_{MZOO}	0.04	0.08	−0.4	+1.6	−2.5	+1.9
TTE	0.09	0.05	−4.5	−2.0	−6.9	−3.8
$EXP_{C,100}$	0.18	0.15	−14.9	−12.7	−14.3	−8.4
$EXP_{C,1500}$	0.04	0.02	−14.9	+0.7	−10.9	+6.0

Note: Because the nitrate is not represented separately in MOD2, z_{nit} is undefined and is denoted by –.

evidence of distributional differences. The strongest distributional response was observed for $O2^{mean}_{0\text{-}600}$. Nevertheless, both the shift in the ensemble median and the uncertainty spread remained small relative to the magnitude of $O2^{mean}_{0\text{-}600}$. The simplified models exhibited narrower uncertainty spreads than FULL, particularly MOD2, for which the uncertainty spread was approxi-
330 mately half that of FULL, as illustrated in Figure 7.

Production-related indicators showed a contrast between primary production and downstream biological pathways. Annual GPP remained close to FULL for both MOD1 and MOD2, while GBP and GSP respond more strongly. For GBP, both MOD1 and MOD2 showed distributional differences from FULL, with a larger K–S statistic D value for MOD2 than for MOD1, and MOD2 also increases the uncertainty spread. For GSP, MOD1 remains close to FULL, whereas MOD2 increases both the
335 median and the uncertainty spread.

Zooplankton-related indicators were more strongly affected in MOD2 than in MOD1. In MOD1, the distributions of $BZOO^{mean}_{0\text{-}600}$ and $BMZOO^{mean}_{0\text{-}600}$ changed slightly and remained close to FULL, with small K–S statistics. In MOD2, however, both distributions shifted towards higher values. Carbon export showed a depth-dependent response, both simplified versions shifted the

https://doi.org/10.5194/egusphere-2026-5134
Preprint. Discussion started: 8 September 2026

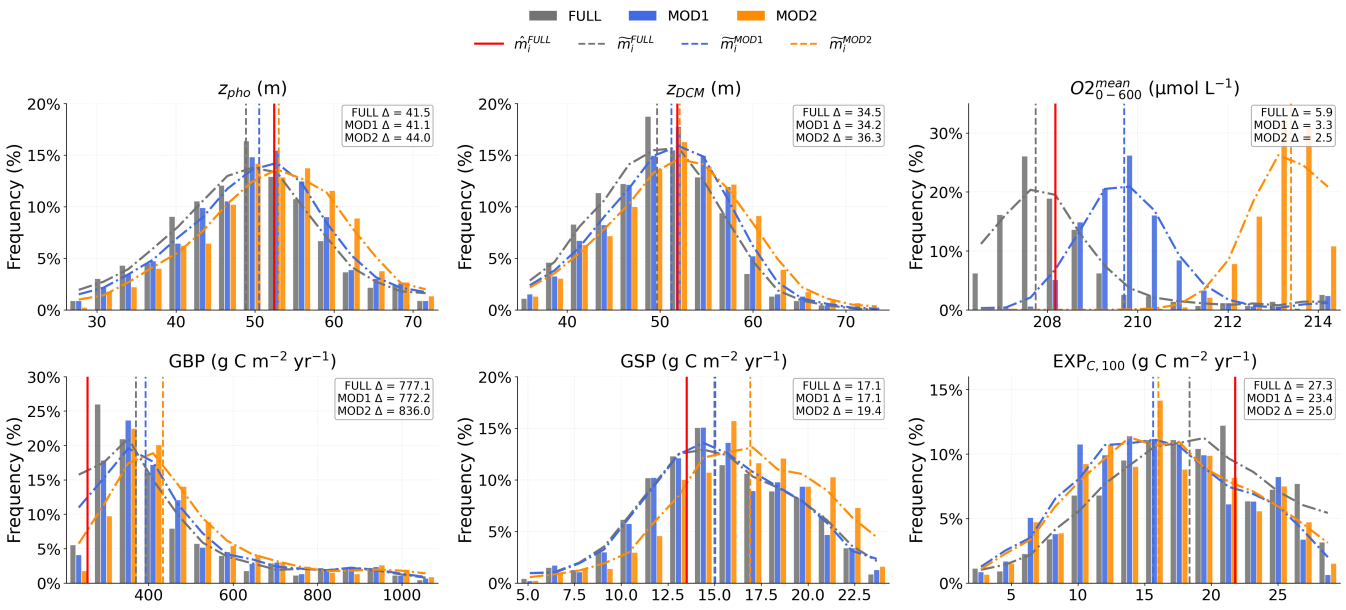

Figure 7. Frequency distributions of selected ecosystem indicators for the FULL (grey), MOD1 (blue), and MOD2 (orange) versions. The red vertical line indicates the FULL reference simulation ($\hat{m}^{\mathrm{FULL}}$), and the dashed vertical lines indicate the ensemble medians ($\widetilde{m}$) of the corresponding versions. The values reported in the upper-right corner indicate the 90% ensemble uncertainty spread Δ.

distribution towards lower values and reduced the uncertainty spread at 100 m. The ensemble median and uncertainty spread of $\mathrm{EXP}_{C,100}$ decreased in both MOD1 and MOD2. These changes are also visible in Figure 7, where the simplified distributions are displaced relative to the FULL version. By contrast, $\mathrm{EXP}_{C,1500}$ showed only small distributional differences from FULL according to the K–S statistic D, although changes in the ensemble median and uncertainty spread were still observed.

4 Discussion

4.1 Distribution of parameter-induced uncertainty in the Eco3M-MED-V1b model

Parameter-induced uncertainty is not uniformly distributed in time or through the water column. Instead, it is concentrated in specific areas of ecological importance, including the upper productive layer, near the nutricline, and the DCM. In time, the uncertainty is mainly concentrated during the spring bloom and the summer stratification period (Fig. 2).

For nutrients, the maximum uncertainty spreads of DIN and PO_4 appear in late summer to autumn at the nutricline depth (70–80 m), corresponding to the period when water column stratification is enhanced, and surface nutrients are depleted. By contrast, although nutrient median concentrations are higher in deeper layers below about 150 m, the associated uncertainty spread remains limited. The maximum uncertainty spread of O_2 also appears at a similar depth, but remains moderate compared with its median value, suggesting that the O_2 is relatively weakly affected by parameter perturbations in biological processes.

https://doi.org/10.5194/egusphere-2026-5134
Preprint. Discussion started: 8 September 2026

This weak relative response may reflect the combined influence of vertical mixing, ventilation, and the large O_2 inventory in the water, which can buffer the effect of biological perturbations. The comparison among these variables shows that uncertainty is higher where biological or biogeochemical processes are most active, not necessarily where the concentrations are highest.

For living organisms, the largest uncertainty spread of BPHY occurs near the surface during the spring bloom (Table 4), where the ensemble median is also high. During the summer–autumn stratified period, the higher median values and uncertainty signal subsequently appeared near the DCM (Fig. 2(b)). The time-depth distribution of BBAC, BUZOO, BMZOO suggest a possible propagation of uncertainty from the primary production to higher trophic levels, and at each trophic level, the uncertainty inherited from the previous level may combine with additional uncertainty caused by the model parameters.

In the model, carbon export is calculated from the sinking flux of DETL. Particle sinking velocities were treated as fixed physical parameters and remained unchanged in the ensemble simulations, their uncertainty was not considered. However, the sinking velocity can depend on particle size or vary with depth, thereby affecting the vertical remineralisation profile and carbon export (Kriest and Oschlies, 2008; Niemeyer et al., 2019). The uncertainty analysed here thus mainly reflects the biogeochemical processes controlling DETL production and loss, including grazing, mortality, faecal-pellet formation, particle hydrolysis, and remineralisation (Boyd and Trull, 2007; Cavan et al., 2017; Steinberg and Landry, 2017). Carbon export uncertainty also integrates the parameter-induced uncertainty propagated through the food web and transferred to DETL.

The distribution of ecosystem indicators provides an integrated view of parameter-induced uncertainty (Fig. 6). In FULL, most indicators are centred around the reference simulation, although their spreads and skewness vary considerably. The O_2 concentration distribution remains relatively narrow, consistent with the weak sensitivity of O_2 to biological perturbation discussed above. In contrast, $\mathrm{BZOO}^{mean}_{0\text{–}600}$, QC_{MZOO}, and $\mathrm{EXP}_{C,100}$ show broader distributions, indicating that the prescribed parameter perturbations lead to a wider range of responses for these indicators. More asymmetric distributions are observed for GBP, $\mathrm{BMZOO}^{mean}_{0\text{–}600}$, and $\mathrm{EXP}_{C,1500}$. For carbon export, the large spread may partly reflect the relatively wide perturbation ranges of uncertain parameters involved in particulate organic matter processing, such as turnover time for DET hydrolysis (τ^{DET}_{hyd}). The strong right-skewness of deep export may also be partly related to its lower bound near zero: some parameter combinations can lead to much higher export, whereas the possible decrease is more limited.

Finally, the FULL ensemble is compared with the DYFAMED observational profiles (Fig. 3) to evaluate its ability to reproduce the mean observed vertical distribution. The ensemble captures the main seasonal and vertical structures of NO_3, PO_4, and Chl, including nutrient depletion in the upper layer, nutricline development, and the DCM. Most observed profiles fall within or close to the ensemble spread. However, some differences remain in regions with strong vertical gradients, particularly near the nutricline and the DCM, and the ensemble spread is generally wider than the observational uncertainty. These differences are at least partly attributable to the 1DV configuration, which simplifies the physical and atmospheric forcing and therefore cannot fully represent the variability of the real system (see Section 2.3).

4.2 Effects of model simplification on ecosystem responses and uncertainty

In general, MOD1 broadly preserves the main time–depth uncertainty distribution of state variables (Fig. 5(a)), whereas MOD2 generally preserves the uncertainty magnitude of ecosystem indicators targeted for the simplification, except the $\mathrm{O2}^{\mathrm{mean}}_{0\text{-}600}$ (Ta-

https://doi.org/10.5194/egusphere-2026-5134
Preprint. Discussion started: 8 September 2026

ble 6(c)). Nevertheless, MOD2 shows more frequent and generally larger distributional deviations from FULL than MOD1. These deviations arise from combined changes in the median, uncertainty spread, and distribution shape (Table 6). For $O2^{\mathrm{mean}}_{0\text{-}600}$, the difference from FULL is mainly associated with a stronger reduction of the uncertainty spread, whereas for $\mathrm{EXP}_{C,100}$, the lower median and reduced spread contribute almost equally.

The time–depth diagnostics help explain these indicator-level differences. MOD2 produces higher BPHY during the early spring bloom, while bloom timing remains broadly similar to that of the FULL model. This suggests that the simplification primarily affects bloom magnitude rather than onset timing, which is mainly governed by light, mixing conditions, and the balance between phytoplankton growth and loss (Behrenfeld et al., 2013; Rumyantseva et al., 2019). Instead, removing these uptake costs increases biomass accumulation and the bloom peak, while accelerating nutrient depletion. Consequently, BPHY declines earlier after the bloom (Fig. 4(b)). This simplification also increases the organic carbon available to bacteria, leading to higher bacterial biomass, these effects then propagate to higher trophic levels, contributing to higher GSP and BZOO in MOD2.

However, carbon export partly differs from this general pattern. $\mathrm{EXP}C,100$ is almost always lower in both simplified versions, while the differences in $\mathrm{EXP}C,1500$ are smaller (Table 6). This can be related to the removal of the MZOO faecal-pellet pathway, which reduces the transfer of grazed carbon to DETL. In MOD2, this decrease is partly compensated during the bloom because the stronger phytoplankton bloom provides more organic matter for mortality and trophic transfer, which can temporarily increase carbon export. The uncertainty response is also different between the two simplified versions. It is mostly reduced in MOD1, while MOD2 shows an increase during the bloom that extends to deeper layers. Near the surface, this uncertainty may be related to changes in BPHY and BBAC during the bloom, while at depth it may also be linked to particle sinking and processing through zooplankton–detritus pathways (Giering et al., 2014). The higher and deeper BBAC in MOD2 may also contribute to the propagation of uncertainty through the microbial food web to zooplankton and deep carbon export (see **S6** in *Supplementary Material*). These results show that model simplification can either reduce or increase carbon export uncertainty, depending on the processes that are simplified or removed.

O_2 shows a different response. Its uncertainty spread decreases by 43.0% in MOD1 and 57.0% in MOD2, which reflects the removal of several biological O_2 source and sink pathways, including zooplankton respiration, photosynthetic O_2 production, growth- and nutrient uptake related O_2 costs, and nitrification-related O_2 consumption (in MOD2). The narrower ensemble therefore reflects a simplified representation of oxygen cycling rather than improved model robustness. Such underestimation could lead to overconfident assessments of ocean deoxygenation and its ecological effects under climate change (Payne et al., 2016; Löptien et al., 2021).

4.3 Integrated ecosystem indicators can mask local uncertainty changes

Integrated ecosystem indicators aggregate responses over time and/or depth and may therefore mask local changes in parameter-induced uncertainty. For example, the phytoplankton related indicators: GPP, $\mathrm{Chl}^{mean}_{surf}$, and DCM_{con} show relatively small changes in their ensemble medians and uncertainty spreads, whereas the time–depth diagnostics reveal BPHY differences that vary in sign across time and depths (Figs. 4 and 5). Agreement in annual GPP or surface Chl may thus result from compensat-

https://doi.org/10.5194/egusphere-2026-5134
Preprint. Discussion started: 8 September 2026

ing local differences during the spring bloom, the stratified period, and around the DCM. To better describe the phytoplankton dynamics therefore require multiple indicators or diagnostics that retain temporal-vertical variability.

Carbon export provides another example. Although $\mathrm{EXP}_{C,100}$ differs from FULL in both simplified versions, with lower median values and reduced uncertainty spread (Table 6), the time–depth diagnostics EXP_{C} showed local positive differences in MOD2 during the bloom and a deeper extension of the positive uncertainty signal (Figs. 4 and 5). For $\mathrm{EXP}_{C,1500}$, the K–S statistic remained small, although changes in the median and spread remain visible, especially in MOD2. Because the $\mathrm{EXP}_{C,1500}$ distribution was highly skewed and small in value (Fig. 6), changes in the percentile-based uncertainty spread (*cf.* Eq. 3) should be interpreted cautiously.

Moreover, previous ensemble studies have shown that parameter-induced uncertainty can vary across time, space, and model outputs (Fiechter, 2012; Mamnun et al., 2022), while the uncertainty and observational constraints of marine ecosystem indicators can also differ considerably among indicators (Skákala et al., 2024; Ciavatta et al., 2025).Building on these studies, we examine whether model simplification can preserve the uncertainty characteristics of the FULL model. Our results show that MOD2 generally preserves the uncertainty magnitude of most targeted ecosystem indicators, but model simplification can still introduce localized changes in time and depth that are not captured by these indicators. For example, the phytoplankton bloom magnitude and its local time–depth evolution changed in MOD2, although these changes were not explicitly represented by the selected indicators. Complementary indicators could therefore include the timing and duration of nutrient depletion, the lag between phytoplankton and zooplankton biomass peaks, carbon export efficiency, and the minimum O_2 concentration and its depth.

The indicators used to guide the construction and evaluation of simplified models should be defined *a priori* according to the specific scientific question and intended application (Planque et al., 2022). In this study, we further suggest that uncertainty analysis can help identify sensitive features that were not initially considered but may be useful as complementary indicators/diagnostics. This principle also applies to the selection of target outputs and validation criteria in surrogate modelling, as discussed below.

4.4 Implications for surrogate model design and evaluation

Surrogate models, also known as emulators, are commonly used to approximate computationally expensive models, thereby supporting sensitivity analysis, uncertainty quantification, and scenario exploration at lower computational cost (Sacks et al., 1989; Razavi et al., 2012). Previous studies have also shown that emulators can be designed for specific ecological or management questions. For example, Skákala et al. (2023) developed machine-learning emulators for oxygen anomalies and hypoxia prediction, and Le Roux et al. (2026) used interpretable symbolic regression to emulate a BGC model very similar to the one used in this study, by predicting annual mean primary production directly from yearly or seasonal climate indicators.

For surrogate modelling, an important issue is the choice of target outputs. If the objective is to predict integrated or summary diagnostics, such as annual integrated GPP or z_{pho}, these quantities can be emulated directly without reconstructing complete time–depth fields. However, integrated outputs may be insufficient for representing state variables with strong temporal and vertical structures, such as BPHY and PO_4 concentration, because they may overlook local responses related to the spring

https://doi.org/10.5194/egusphere-2026-5134
Preprint. Discussion started: 8 September 2026

bloom, nutrient limitation, or seasonal biomass redistribution. In such cases, emulators should reproduce the relevant time–depth fields or include more diagnostics that preserve the timing, magnitude, and depth of these local characteristics.

In addition, emulator construction could rely on training data generated from mechanistic model simulations (O'Hagan, 2006). Using simplified model versions to generate part of training dataset is a possible way to reduce computational cost. However, for state variables or ecosystem indicators that are more sensitive to simplification, such as GBP, BMZOO, and EXP_C, directly using a simplified version as a substitute for FULL to construct an emulator may introduce systematic bias. A more robust strategy could be to treat the simplified versions as low-fidelity models and the FULL version as a high-fidelity reference. A large ensemble of simplified model simulations could then be combined with a smaller number of FULL simulations to learn and account for the discrepancy between the two fidelities, for example using Bayesian model-discrepancy approaches (Kennedy and O'Hagan, 2001) or co-kriging-based multi-fidelity surrogate modelling (Forrester et al., 2007; Peherstorfer et al., 2018). A related application of multi-fidelity Gaussian process metamodeling to Eco3M-MED-CN model in 1DV configuration is currently being developed by Saillet (in prep).

4.5 Methodological implications, limitations, and transferability

The UQ experimental design provides a reusable framework for assessing how model simplification affects parameter-induced uncertainty. Beyond quantifying the effects of simplification, it can also be used to determine whether a more complex model produces more robust indicator estimates or better represents local spatio–temporal structures. By applying the same Sobol low-discrepancy ensemble to the 30 parameters shared by FULL, MOD1, and MOD2, differences among the model versions can be attributed more directly to model simplification rather than to differences in sampling. The parameter-induced uncertainty quantified here is therefore conditional on this common set of shared parameters and does not represent the total parametric uncertainty . Sobol sequences provide relatively uniform coverage of multidimensional parameter spaces and are more efficient than Monte Carlo sampling (Saltelli et al., 2010). However, sample size and convergence should still be checked for each application (Sarrazin et al., 2016; Pianosi et al., 2016).

Furthermore, the interpretation of $\phi(\log_{10}\Delta^S)$ (Eq. 4) requires caution, because this metric expresses relative changes in uncertainty spread. Large positive values may therefore occur when the absolute spread in FULL is very small. For example, the strong MOD2 signal near 200 m during the summer–autumn stratified period indicates a local relative increase in uncertainty spread, but not necessarily a large absolute uncertainty. This metric is useful for detecting changes in the relative uncertainty structure, but it should be interpreted together with absolute spread differences values, ensemble medians, and the magnitude of the underlying state variable. Its interpretation also depends on how ensemble uncertainty is summarised. Here, the 5%–95% quantile range limits the influence of extreme parameter combinations, including simulations with near-zero biological activity (see **S4** in *Supplementary Material*), but it may also mask rare and extreme responses.

Finally, this study is based on a 1DV configuration at the DYFAMED station, the uncertainty patterns identified here should therefore be tested under more complex and realistic physical conditions. A natural extension would be to apply the same uncertainty quantification framework to 3D model configurations, potentially using surrogate models to reduce computational

https://doi.org/10.5194/egusphere-2026-5134
Preprint. Discussion started: 8 September 2026

costs. For example, Hemmings et al. (2015) developed a site-based mechanistic emulator that used low-cost 1D simulations to generate rapid probabilistic estimates for a target 3D BGC model, supporting parameter analysis and model calibration.

5 Conclusions

This study quantified parameter-induced uncertainty of marine biogeochemical model Eco3M-MED-V1b in 1DV configuration and examined how this uncertainty was modified by two simplified model versions. Applying the same Sobol low-discrepancy parameter ensemble to all three model versions (FULL, MOD1, and MOD2) enabled direct comparisons under identical parameter perturbations. Parameter-induced uncertainty in FULL version was not uniformly distributed, but concentrated in ecologically meaningful periods and depth, including the spring bloom, the summer stratification period, the upper productive layer, the nutricline, and the DCM. Simplification affected the ensemble median and uncertainty spread in a strongly process-dependent way. MOD1 broadly preserved the main time–depth uncertainty distribution of the selected state variables, whereas MOD2 generally preserved the uncertainty magnitude of the ecosystem indicators targeted for simplification. However, the level of fidelity varied among diagnostics. Moreover, O_2 uncertainty was strongly reduced because several biological source and sink pathways were removed, rather than because the simplified models were more robust. Carbon export uncertainty could either decrease or increase depending on the processes removed and their role along the export pathway.

Similar uncertainty magnitudes in indicators integrated over the whole year or water column may nevertheless mask differences that appear when the same indicators are examined over specific periods or depth ranges. Target diagnostics for model simplification and model evaluation criteria should therefore be defined *a priori* according to the specific scientific question and intended application. Uncertainty analysis can also help identify complementary indicators/diagnostics, such as phytoplankton bloom timing and intensity. Further work could extend this framework to 3D model configurations and combine it with emulation, multi-fidelity surrogate modelling, or observational calibration to evaluate the robustness of model simplification under more realistic physical conditions and parameter constraints.

Code and data availability. The source code of the Eco3M modular modelling platform is available on GitHub at https://github.com/Eco3M/Eco3M. The DYFAMED observational data were obtained from the publicly available dataset at https://www.seanoe.org/data/00326/43749/.

Appendix A: Parameter uncertainty setup and sampling strategy

A1 Parameter reference values and literature-based intervals

For each model parameter p_i, a reference value p_i^{ref} is first defined based on the available literature and expert judgement. Available values and ranges reported in the literature are summarised in Table B1. Based on this information and expert judgement, a numerical literature-informed interval is defined as

$$\Phi_{i,\mathrm{lit}} = (L_{i,\mathrm{lit}}, U_{i,\mathrm{lit}}),$$

https://doi.org/10.5194/egusphere-2026-5134
Preprint. Discussion started: 8 September 2026

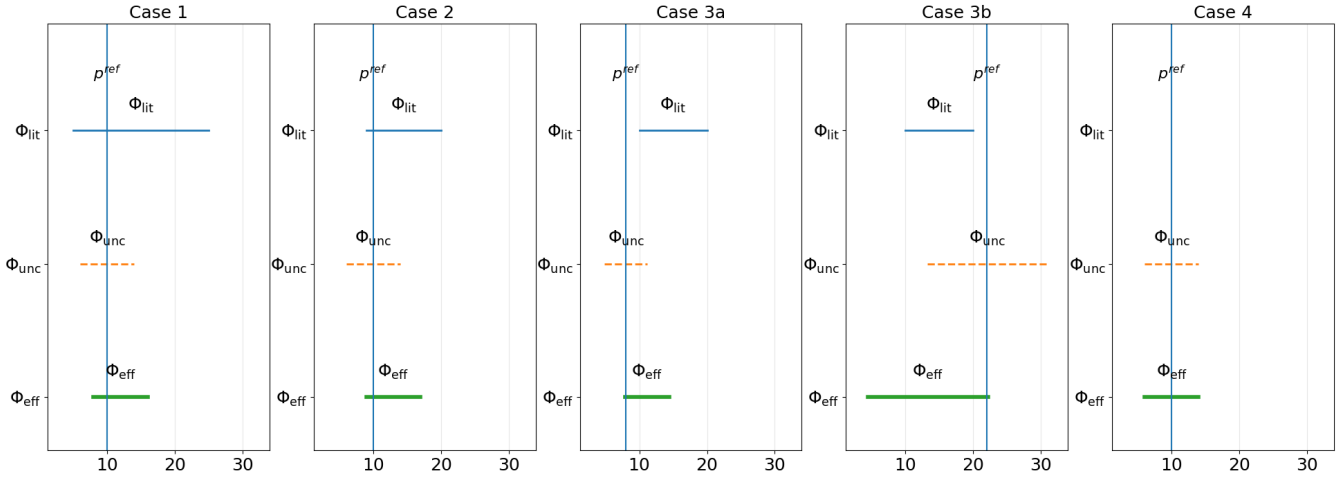

Figure A1. Schematic illustration of the rules used to construct the $\Phi_{i,\mathrm{eff}}$.

where $L_{i,\mathrm{lit}}$ and $U_{i,\mathrm{lit}}$ denote the minimum and maximum values, respectively.

In some cases, the reference value p_i^{ref} may be close to the bound of $\Phi_{i,\mathrm{lit}}$ or even lie outside this interval. In the present study, p_i^{ref} serves as the mode of the Beta distribution (details are provided in A4). An effective interval $\Phi_{i,\mathrm{eff}}$ used by UQ is then constructed based on $\Phi_{i,\mathrm{lit}}$ and the position of p_i^{ref} relative to $\Phi_{i,\mathrm{lit}}$ (details see A3).

A2 Symmetric uncertainty interval around the reference value

The parameter categories and uncertainty factor f_i are defined in Section 2.3.1 and Eq. 1. Using f_i, a symmetric uncertainty interval $\Phi_{i,\mathrm{unc}}$ is defined around the model reference value:

$$\Phi_{i,\mathrm{unc}} = \left(p_i^{ref} - f_i p_i^{ref},\ p_i^{ref} + f_i p_i^{ref}\right) \tag{A1}$$

The width of this interval is

$$W_{i,\mathrm{unc}} = 2 f_i p_i^{ref} \tag{A2}$$

Accordingly, the interval width equals $0.4p_i^{ref}$, $0.8p_i^{ref}$, and $1.6p_i^{ref}$ for WC, MC, and UC parameters, respectively.

A3 Construction of the effective uncertainty interval

The effective sampling interval

$$\Phi_{i,\mathrm{eff}} = (L_{i,\mathrm{eff}}, U_{i,\mathrm{eff}}) \tag{A3}$$

is constructed by combining the $\Phi_{i,\mathrm{unc}}$ and the $\Phi_{i,\mathrm{lit}}$. Four cases are considered in this study (see Fig. A1).

https://doi.org/10.5194/egusphere-2026-5134
Preprint. Discussion started: 8 September 2026

A3.1 Case 1: $\Phi_{i,\mathrm{unc}} \subset \Phi_{i,\mathrm{lit}}$.

The relative position of p_i^{ref} within $\Phi_{i,\mathrm{lit}}$ is defined as

$$r_i = \frac{p_i^{ref} - L_{i,\mathrm{lit}}}{U_{i,\mathrm{lit}} - L_{i,\mathrm{lit}}}, \qquad W_{i,\mathrm{eff}} = W_{i,\mathrm{unc}} = 2 f_i p_i^{ref} \tag{A4}$$

The interval is translated without changing its width:

$$L_{i,\mathrm{eff}} = p_i^{ref} - r_i W_{i,\mathrm{unc}}, \qquad U_{i,\mathrm{eff}} = L_{i,\mathrm{eff}} + W_{i,\mathrm{unc}} \tag{A5}$$

A3.2 Case 2: $p_i^{ref} \in \Phi_{i,\mathrm{lit}}$ but $\Phi_{i,\mathrm{unc}} \not\subseteq \Phi_{i,\mathrm{lit}}$.

$\Phi_{i,\mathrm{eff}}$ is located at the nearest bound of $\Phi_{i,\mathrm{lit}}$ and extended in the opposite direction with maximum width $W_{i,\mathrm{unc}}$:

$$\text{if } (p_i^{ref} - L_{i,\mathrm{lit}}) \le (U_{i,\mathrm{lit}} - p_i^{ref}): \quad L_{i,\mathrm{eff}} = L_{i,\mathrm{lit}},\ U_{i,\mathrm{eff}} = L_{i,\mathrm{lit}} + W_{i,\mathrm{unc}} \tag{A6}$$

$$\text{otherwise}: \quad U_{i,\mathrm{eff}} = U_{i,\mathrm{lit}},\ L_{i,\mathrm{eff}} = U_{i,\mathrm{lit}} - W_{i,\mathrm{unc}}. \tag{A7}$$

A3.3 Case 3: $p_i^{ref} \notin (L_{i,\mathrm{lit}}, U_{i,\mathrm{lit}})$ or p_i^{ref} lies exactly on a bound.

We keep p_i^{ref} as the mode value of the Beta distribution, but we avoid having p_i^{ref} exactly at a bound of $\Phi_{i,\mathrm{eff}}$ to reduce boundary effects. A very small margin is introduced by setting $\varepsilon = 0.01$ and $\delta_i = \varepsilon p_i^{ref}$. The $\Phi_{i,\mathrm{eff}}$ is then oriented toward the domain of $\Phi_{i,\mathrm{lit}}$:

- Case 3a: If $p_i^{ref} \le L_{i,\mathrm{lit}}$ (reference below the $\Phi_{i,\mathrm{lit}}$ minimum),

$$L_{i,\mathrm{eff}} = p_i^{ref} - \delta_i, \qquad U_{i,\mathrm{eff}} = p_i^{ref} + W_{i,\mathrm{unc}} \tag{A8}$$

- Case 3b: If $p_i^{ref} \ge U_{i,\mathrm{lit}}$ (reference above the $\Phi_{i,\mathrm{lit}}$ maximum),

$$U_{i,\mathrm{eff}} = p_i^{ref} + \delta_i, \qquad L_{i,\mathrm{eff}} = p_i^{ref} - W_{i,\mathrm{unc}} \tag{A9}$$

A3.4 Case 4: no $\Phi_{i,\mathrm{lit}}$ is available.

When $\Phi_{i,\mathrm{lit}}$ is not available, we simply set

$$\Phi_{i,\mathrm{eff}} = \Phi_{i,\mathrm{unc}} \tag{A10}$$

Note: In Cases 2 and 3, additional validity constraints may be required (e.g. ratios parameters should be bounded in $(0,1)$). In the present study, such situations did not occur, but one should be aware of other case studies.

https://doi.org/10.5194/egusphere-2026-5134
Preprint. Discussion started: 8 September 2026

A4 Beta distribution setting and sampling

For $X_i \sim \mathrm{Beta}(\alpha_i, \beta_i)$ with $\alpha_i, \beta_i > 1$, the mode value and concentration is given by (details in Ferrari and Cribari-Neto (2004); Kruschke (2014))

$$\omega_i = \frac{\alpha_i - 1}{\alpha_i + \beta_i - 2}, \qquad \kappa_i = \alpha_i + \beta_i \tag{A11}$$

The scaled mode value corresponding to the reference value (p_i^{ref}) in $\Phi_{i,\mathrm{eff}}$ defined as :

$$\omega_i = \frac{p_i^{\mathrm{ref}} - L_{i,\mathrm{eff}}}{U_{i,\mathrm{eff}} - L_{i,\mathrm{eff}}} \in (0,1). \tag{A12}$$

We adopt the mode–concentration parametrisation:

$$\alpha_i = 1 + (\kappa_i - 2)\omega_i, \qquad \beta_i = 1 + (\kappa_i - 2)(1 - \omega_i), \tag{A13}$$

where $\kappa_i > 2$ controls concentration: larger κ_i yields a distribution more concentrated around the mode.

A4.1 Parameter sampling distribution

For parameters that have the $\Phi_{i,\mathrm{lit}}$, we sample p_i using a bounded Beta distribution over $\Phi_{i,\mathrm{eff}}$, with the mode ω_i defined in Eq. (A12). For parameters without $\Phi_{i,\mathrm{lit}}$ (Case 4 in A), we use a uniform distribution over $\Phi_{i,\mathrm{unc}}$ ($\kappa = 2$ for Beta distribution).

A4.2 Choice of the concentration κ_i for beta distribution

In this study, a simple group-consistent choice is adopted:

$$\kappa_i = \max\left(20 \cdot \frac{W_{i,\mathrm{eff}}}{W_{i,\mathrm{lit}}}, 2\right). \tag{A14}$$

We use $\kappa = 20$ as the default value, since it yields a distribution clearly centred on the mode while maintaining non-negligible variability. In this case, the κ_i is governed by the relative magnitudes of $\Phi_{i,\mathrm{eff}}$ to $\Phi_{i,\mathrm{lit}}$.

Appendix B: Parameter ranges in the literature

We summarised the ranges of model parameters based on the literature and expert judgement. Table B1 summarises the reference values used in the model, the ranges derived from the literature ($\Phi_{i,\mathrm{lit}}$), the effective ranges adopted for UQ ($\Phi_{i,\mathrm{eff}}$), the parameter groups, sampling distribution, literature references, and brief descriptions of each parameter. Moreover, Figure. B1 illustrates the actual parameter distributions obtained by mapping 512 Sobol sequence samples onto $\Phi_{i,\mathrm{eff}}$. Note that $\Phi_{i,\mathrm{eff}}$ represents the prescribed sampling range. Because the finite Sobol sequence ensemble does not necessarily sample the exact interval bounds, the final realised parameter range shown in Fig. B1 may be narrower than $\Phi_{i,\mathrm{eff}}$.

https://doi.org/10.5194/egusphere-2026-5134
Preprint. Discussion started: 8 September 2026

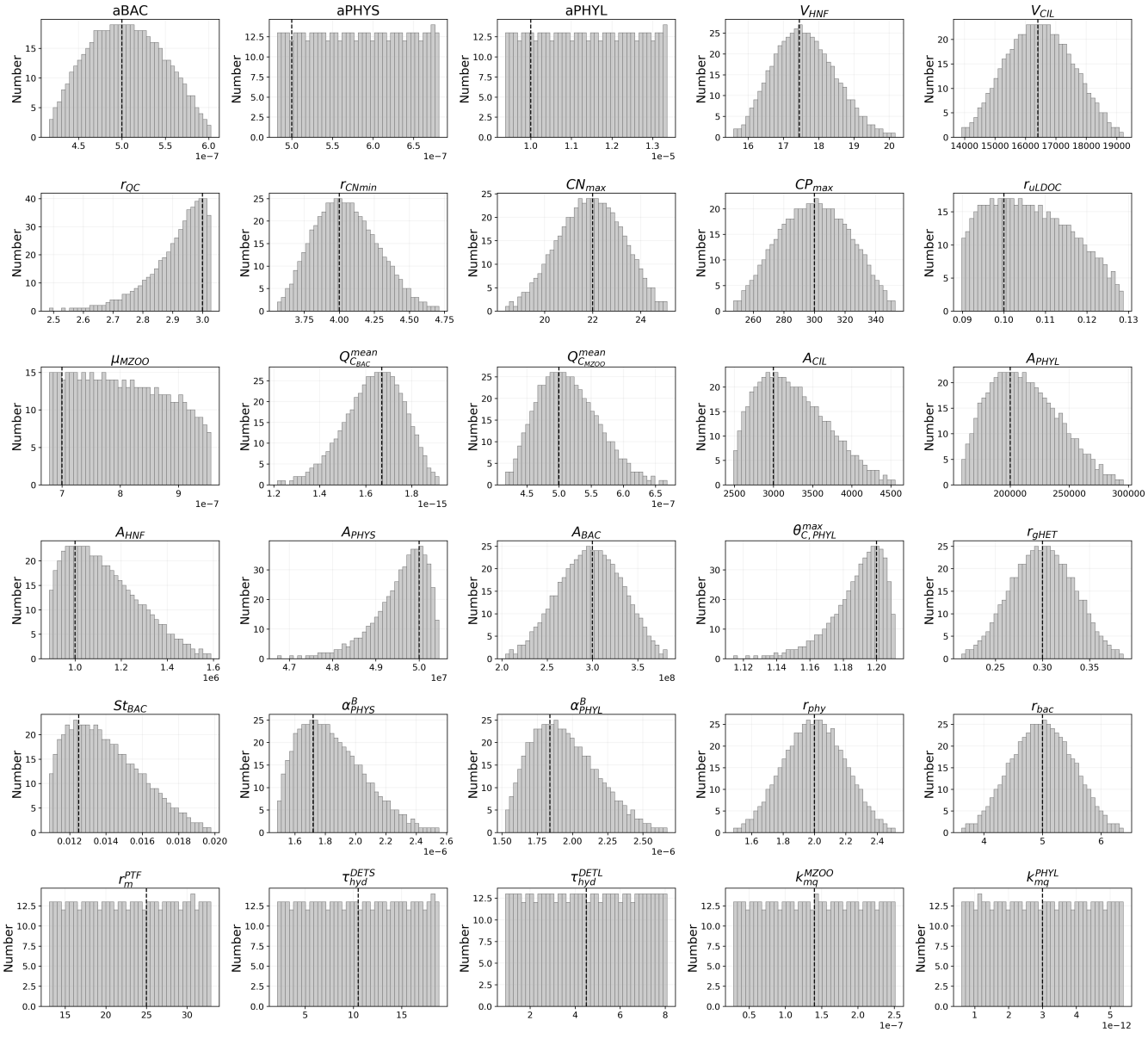

Figure B1. Histogram of parameter distributions (N = 512), obtained by Sobol sequence sampling and mapping to $\Phi_{i,\mathrm{eff}}$. The dashed vertical lines indicate the parameter reference values. The meaning of parameter symbols can be found in Table B1.

https://doi.org/10.5194/egusphere-2026-5134
Preprint. Discussion started: 8 September 2026

Table B1. Details of the parameters used in the uncertainty quantification and the literature references. The *Literature values* column reports values available in the literature, while $\Phi_{i,\mathrm{lit}}$ denotes the numerical interval defined based on literature information and expert judgement and used for the $\Phi_{i,\mathrm{eff}}$ construction. $\Phi_{i,\mathrm{eff}}$ denotes the resulting effective sampling interval. The cases refer to the interval construction rules illustrated in Fig. A1.

Parameter	p_i^{ref}	Unit	Literature values	$\Phi_{i,\mathrm{lit}}$	$\Phi_{i,\mathrm{eff}}$	Case	Grp./Distri.	Reference	Description
H_{BAC}	0.5	μm	0.115–1.875	0.1–1.0	0.41–0.61	1	WC/Beta	La Ferla et al. (2004)	Semi-major axis of BAC cells.
			0.075–0.5					Andersen et al. (2016)	
H_{PHYS}	0.5	μm	0.3–1.0	0.3–2.5	0.48–0.68	1	WC/Beta	Irwin et al. (2006)	Semi-major axis of PHYS cells.
H_{PHYL}	10.0	μm	> 2	2.5–50	9.37–13.37	1	WC/Beta	Leblanc et al. (2018)	Semi-major axis of PHYL cells.
V_{HNF}	17.4	$\mu\mathrm{m}^3$	15.2–26.2	15–25	15.0–21.98	2	WC/Beta	Tanaka and Rassoulzadegan (2002)	HNF cell volume.
V_{CIL}	$1.64\,10^4$	$\mu\mathrm{m}^3$	$8.9\,10^3$–$2.4\,10^4$	$9.0\,10^3$–$2.5\,10^4$	$1.34\,10^4$–$1.99\,10^4$	1	WC/Beta	Tanaka and Rassoulzadegan (2002)	CIL cell volume.
r_{QC}	3.0	–	1.1–3.0	1.1–3.0	1.80–3.03	3b	WC/Beta	Liefer et al. (2019)	Carbon quota ratio.
r_{CNmin}	4.0	mol C (mol N)$^{-1}$	4.0	3.0–6.0	3.47–5.07	1	WC/Beta	Geider and La Roche (2002)	Minimum C:N quota ratio in organisms.
			~ 3 (protein-based)					Liefer et al. (2019)	
CN_{max}	22.0	–	17.0	12–30	17.11–25.91	1	WC/Beta	Geider and La Roche (2002)	Maximum C:N ratio.
			12.2–51.6					Liefer et al. (2019)	
CP_{max}	300.0	mol C (mol P)$^{-1}$	135.0	100–500	240–360	1	WC/Beta	Geider and La Roche (2002)	Maximum C:P ratio.
			100–238					Liefer et al. (2019)	
r_{uLDOC}	0.1	–	0.104	0.03–0.30	0.09–0.13	1	WC/Beta	Eiler et al. (2003)	Energetic cost proxy of LDOC assimilation.
			0.19–0.39					Tanaka and Rassoulzadegan (2004)	
			0.03–0.31					Sempéré et al. (2000)	
μ_{MZOO}	$7\,10^{-7}$	s^{-1}	0.01–0.27 day^{-1} [(a)]	$5\,10^{-7}$–$3\,10^{-6}$	$6.78\,10^{-7}$–$9.58\,10^{-7}$	1	WC/Beta	Richardson and Verheye (1998)	Maximum specific growth rate of MZOO.
			$1.1\,10^{-4}$–$6.9\,10^{-4}$ (egg fem^{-1} s^{-1})					Halsband-Lenk et al. (2004)	

https://doi.org/10.5194/egusphere-2026-5134
Preprint. Discussion started: 8 September 2026

Table B1 (continued)

Parameter	p_i^{ref}	Unit	Literature values	$\Phi_{i,\mathrm{lit}}$	$\Phi_{i,\mathrm{eff}}$	Case	Grp./Distri.	Reference	Description
$Q_{C_{MZOO}}^{mean}$	$5.0\ 10^{-7}$	mol C ind^{-1}	$3.7\ 10^{-8}$–$5.4\ 10^{-6}$ $4.2\ 10^{-7}$–$1.25\ 10^{-6}$ (females)	$4\ 10^{-7}$–$1\ 10^{-6}$	$4\ 10^{-7}$–$8\ 10^{-7}$	2	MC/Beta	Landry et al. (2001) Halsband-Lenk et al. (2004)	Mean intracellular C quota of MZOO.
$Q_{C_{BAC}}^{mean}$	$1.67\ 10^{-15}$	mol C cell^{-1}	15.0–26.0 fg C cell^{-1} [(b)] 20.0 fg C cell^{-1} [(b)] 26.0 fg C cell^{-1} (starvation state) [(b)]	$1\ 10^{-15}$–$2\ 10^{-15}$	$6.64\ 10^{-16}$–$2.0\ 10^{-15}$	2	MC/Beta	Caron et al. (1995) Lee and Fuhrman (1987) Trousselier et al. (1997)	Mean intracellular C quota of BAC.
A_{CIL}	$3.0\ 10^{3}$	cell L^{-1}	$1.0\ 10^{3}$–$1.0\ 10^{4}$ up to $1.0\ 10^{4}$ up to $1.5\ 10^{4}$	$1\ 10^{3}$–$1\ 10^{4}$	$2.47\ 10^{3}$–$4.87\ 10^{3}$	1	MC/Beta	Quevedo and Anadon (2000) Pérez et al. (2000) Tanaka and Rassoulzadegan (2002)	Typical abundance of CIL.
A_{PHYS}	$5.0\ 10^{7}$	cell L^{-1}	$1.0\ 10^{6}$–$1.0\ 10^{8}$ $1.0\ 10^{5}$–$1.0\ 10^{7}$	$1\ 10^{6}$–$1\ 10^{7}$	$1\ 10^{7}$–$5.05\ 10^{7}$	3b	MC/Beta	Jacquet et al. (2002) Christaki et al. (2001)	Typical abundance of PHYS.
A_{PHYL}	$2.0\ 10^{5}$	cell L^{-1}	$> 1.0\ 10^{5}$	$5\ 10^{4}$–$6\ 10^{5}$	$1.56\ 10^{5}$–$3.16\ 10^{5}$	1	MC/Beta	Percopo et al. (2011)	Typical abundance of PHYL.
A_{HNF}	$1.0\ 10^{6}$	cell L^{-1}	$4.2\ 10^{2}$–$4.65\ 10^{3}$ cell mL^{-1} [(c)] $1.0\ 10^{2}$–$1.0\ 10^{3}$ cell mL^{-1} (Surface) [(c)] $1.0\ 10^{2}$–$1.2\ 10^{3}$ cell mL^{-1} [(c)]	$5\ 10^{5}$–$4\ 10^{6}$	$8.86\ 10^{5}$–$1.69\ 10^{6}$	1	MC/Beta	Christaki et al. (2011) Vázquez-Domínguez et al. (2008) Tanaka and Rassoulzadegan (2002)	Typical abundance of HNF.
A_{BAC}	$3.0\ 10^{8}$	cell L^{-1}	$5.0\ 10^{7}$–$11.5\ 10^{8}$ $4.3\ 10^{7}$–$4.4\ 10^{8}$ (mesopelagic layer)	$5\ 10^{7}$–$5\ 10^{8}$	$1.67\ 10^{8}$–$4.07\ 10^{8}$	1	MC/Beta	Pulido-Villena et al. (2008) Tanaka and Rassoulzadegan (2004)	Typical abundance of BAC.

https://doi.org/10.5194/egusphere-2026-5134
Preprint. Discussion started: 8 September 2026

Table B1 (continued)

Parameter	p_i^{ref}	Unit	Literature values	$\Phi_{i,\mathrm{lit}}$	$\Phi_{i,\mathrm{eff}}$	Case	Grp./Distri.	Reference	Description
$\theta_{C,PHYL}^{max}$	1.2	g Chl mol C^{-1}	0.01–0.08 mg Chl mg C^{-1} [(d)]	0.96–1.20	0.24–1.21	3b	MC/Beta	Geider (1987)	Maximum chlorophyll-to-carbon ratio.
			< 0.12 to > 0.96 g Chl mol C^{-1}					Faure et al. (2006)	
			0.4–0.6 g Chl mol C^{-1} (DCM)					Marañón et al. (2021)	
Parameter $\theta_{C,PHYS}^{max}$ is the same value as $\theta_{C,PHYL}^{max}$.									
St_{BAC}	0.0125	–	$4.8\ 10^{-3}$–$4.8\ 10^{-2}$	0.005–0.05	0.01–0.02	1	MC/Beta	Aksnes and Cao (2011)	Fraction of BAC surface covered by uptake sites.
This parameter is also used to derive the fraction of PHYL/PHYS surface covered by uptake sites through a fixed ratio.									
α_{PHYS}^{B}	$1.72\ 10^{-6}$ mol C m^2 gChl^{-1} J^{-1}		0.033–0.049 [*(e)]	$1\ 10^{-6}$–$5\ 10^{-6}$	$1.47\ 10^{-6}$–$2.85\ 10^{-6}$	1	MC/Beta	Richardson et al. (2016)	Initial light-limited slope for PHYS.
			0.021–0.028 [*(e)] (pico-phytoplankton)					Robinson et al. (2018)	
			0.005–0.040 [*(e)] (seasonal means)					Kulk et al. (2020)	
***Unit in literature:** mgC (mg Chl)$^{-1}$ h^{-1} (μmol photons m^{-2} s^{-1})$^{-1}$									
α_{PHYL}^{B}	$1.84\ 10^{-6}$ mol C m^2 gChl^{-1} J^{-1}		0.019–0.033 [*(e)]	$1.50\ 10^{-6}$–$5.50\ 10^{-6}$	$1.50\ 10^{-6}$–$2.97\ 10^{-6}$	2	MC/Beta	Richardson et al. (2016)	Initial light-limited slope for PHYL.
			0.017–0.052 [*(e)] (micro+nano-phytoplankton)					Robinson et al. (2018)	
			0.005–0.040 [*(e)] (seasonal means)					Kulk et al. (2020)	
***Unit in literature:** mgC (mg Chl)$^{-1}$ h^{-1} (μmol photons m^{-2} s^{-1})$^{-1}$									
r_{gHET}	0.3	–	0.35	0.10–0.50	0.18–0.42	1	MC/Beta	Šimek et al. (1996)	Energy cost for heterotroph growth.
			0.2–0.3					Chen et al. (2010)	
			0.3–0.5					Verity et al. (1999)	
r_{phy}	2.0	–	1.0–3.0	1.0–3.0	1.2–2.8	1	MC/Beta	Clavano et al. (2007)	Major/minor axis ratio for phytoplankton cells.
r_{bac}	5.0	–	2.0–8.0	2.0–8.0	3.0–7.0	1	MC/Beta	La Ferla et al. (2004)	Major/minor axis ratio for bacterial cells.
			4.5–5.3					Maimone et al. (2023) (curved rods)	
r_m^{PFT}	25.0	–	–	10.0–35.0	13.0–33.0	4	MC/Uniform	expert judgment	Ratio between specific growth and mortality rates of PFTs.

https://doi.org/10.5194/egusphere-2026-5134
Preprint. Discussion started: 8 September 2026

Table B1 (continued)

Parameter	p_i^{ref}	Unit	Literature values	$\Phi_{i,\mathrm{lit}}$	$\Phi_{i,\mathrm{eff}}$	Case	Grp./Distri.	Reference	Description
τ_{hyd}^{DETS}	10.5	day	–	2.1–18.9	2.1–18.9	4	UC/Uniform	expert judgment	Turnover time for DETS hydrolysis.
τ_{hyd}^{DETL}	4.5	day	–	0.9–8.1	0.9–8.1	4	UC/Uniform	expert judgment	Turnover time for DETL hydrolysis
k_{mq}^{MZOO}	$1.4\,10^{-7}$	$\mathrm{ind}^{-1}\mathrm{s}^{-1}$	–	$2.80\,10^{-8}$–$2.52\,10^{-7}$	$2.80\,10^{-8}$–$2.52\,10^{-7}$	4	UC/Uniform	expert judgment	Quadratic mortality rate of MZOO.
k_{mq}^{PHYL}	$3.0\,10^{-12}$	$\mathrm{cell}^{-1}\mathrm{s}^{-1}$	–	$6.0\,10^{-13}$–$5.4\,10^{-12}$	$6.0\,10^{-13}$–$5.4\,10^{-12}$	4	UC/Uniform	expert judgment	Quadratic mortality rate of PHYL.

Notes on unit conversion for Table B1

[a] $\mathrm{day}^{-1} \rightarrow \mathrm{s}^{-1}$: divide by 86400.

[b] fg C $\mathrm{cell}^{-1} \rightarrow$ mol C cell^{-1}: $(\mathrm{fg}\ 10^{-15})/12$.

[c] cell $\mathrm{mL}^{-1} \rightarrow$ cell L^{-1}: multiply by 10^3.

[d] mg Chl mg $\mathrm{C}^{-1} \rightarrow$ g Chl mol C^{-1}: multiply by 12.

[e] $\alpha_{\mathrm{lit}}^{B}$ defined in $\mathrm{mg\,C\,(mg\,Chl\,a)^{-1}\,h^{-1}\,(\mu mol\,photons\,m^{-2}\,s^{-1})^{-1}}$ in the literature, is converted to the unit in the model ($\mathrm{mol\,C\,m^2\,gChl^{-1}\,J^{-1}}$) by $\alpha_{\mathrm{model}}^{B} = \alpha_{\mathrm{lit}}^{B} \times \frac{1}{12\times3600\times0.217}$; with mol C (mol photons)$^{-1} \rightarrow$ mol C J^{-1}: divide by $2.17\ 10^5$ (using μmol photons $\approx 0.217J$).

Author contributions. **Yutong Zhang:** Conceptualization, Investigation, Formal analysis, Methodology, Validation, Visualization, Writing (original draft preparation), Writing (review and editing); **Pierre Brasseur:** Conceptualization, Methodology, Supervision, Funding acquisition, Writing (review and editing); **Melika Baklouti:** Conceptualization, Model development, Methodology, Supervision, Funding acquisition, Writing (review and editing); **Jean-Michel Brankart:** Conceptualization, Methodology, Writing (review and editing).

Competing interests. The authors declare that they have no conflict of interest.

Acknowledgements. This research is part of the doctoral work of Yutong ZHANG at Mediterranean Institute of Oceanography (Aix-Marseille university), in collaboration with the Institute of Environmental Geosciences within the MEDIATION project. The project received funding from the French National Research Agency (ANR) under the France 2030 initiative, through the *"Océans et Climat"* programme (ANR-22-POCE-0003). The high-performance computing (HPC) resources of GENCI-IDRIS (grant No. 2018-0227) made it possible to verify, prior to this study, the fidelity of the simplified models at the Mediterranean basin scale (in 3D configuration).

Use of generative AI tools. During the preparation of this manuscript, the author used ChatGPT to improve the readability and language of the manuscript and to assist with LaTeX typesetting and table formatting. After using this tool, the author reviewed and edited the content as needed and takes full responsibility for the content of the published article.

https://doi.org/10.5194/egusphere-2026-5134
Preprint. Discussion started: 8 September 2026

References

Aksnes, D. L. and Cao, F. J.: Inherent and apparent traits in microbial nutrient uptake, Marine ecology progress series, 440, 41–51, https://doi.org/10.3354/meps09355, 2011.

Andersen, K., Berge, T., Gonçalves, R., Hartvig, M., Heuschele, J., Hylander, S., Jacobsen, N., Lindemann, C., Martens, E., Neuheimer, A., Olsson, K., Palacz, A., Prowe, A., Sainmont, J., Traving, S., Visser, A., Wadhwa, N., and Kiørboe, T.: Characteristic Sizes of Life in the Oceans, from Bacteria to Whales*, Annual Review of Marine Science, 8, 217–241, https://doi.org/10.1146/annurev-marine-122414-034144, 2016.

Anugerahanti, P., Roy, S., and Haines, K.: A perturbed biogeochemistry model ensemble evaluated against in situ and satellite observations, Biogeosciences, 15, 6685–6711, https://doi.org/10.5194/bg-15-6685-2018, 2018.

Aumont, O., Ethé, C., Tagliabue, A., Bopp, L., and Gehlen, M.: PISCES-v2: an ocean biogeochemical model for carbon and ecosystem studies, Geoscientific Model Development, 8, 2465–2513, https://doi.org/10.5194/gmd-8-2465-2015, 2015.

Baklouti, M., Faure, V., Pawlowski, L., and Sciandra, A.: Investigation and sensitivity analysis of a mechanistic phytoplankton model implemented in a new modular numerical tool (Eco3M) dedicated to biogeochemical modelling, *Progress in Oceanography*, 71(1), 34–58, https://doi.org/10.1016/j.pocean.2006.05.003, 2006.

Baklouti, M., Pagès, R., Alekseenko, E., Guyennon, A., and Grégori, G.: On the benefits of using cell quotas in addition to intracellular elemental ratios in flexible-stoichiometry Plankton functional type models. Application to the Mediterranean Sea, *Progress in Oceanography*, 197, 102 634, https://doi.org/10.1016/j.pocean.2021.102634, 2021.

Baklouti, M., Zhang, Y., Mazoyer, C., Barrier, N., and Pagès, R.: A New Method for Consistent and Simplified Parameterization of Marine Biogeochemical Models: Application to the Eco3M-MED V2 Model in the Mediterranean Sea, manuscript submitted to Journal of Advances in Modeling Earth Systems, under review.

Behrenfeld, M. J., Doney, S. C., Lima, I., Boss, E. S., and Siegel, D. A.: Annual cycles of ecological disturbance and recovery underlying the subarctic Atlantic spring plankton bloom, Global Biogeochemical Cycles, 27, 526–540, https://doi.org/10.1002/gbc.20050, 2013.

Bopp, L., Resplandy, L., Orr, J. C., Doney, S. C., Dunne, J. P., Gehlen, M., Halloran, P., Heinze, C., Ilyina, T., Séférian, R., Tjiputra, J., and Vichi, M.: Multiple stressors of ocean ecosystems in the 21st century: projections with CMIP5 models, Biogeosciences, 10, 6225–6245, https://doi.org/10.5194/bg-10-6225-2013, 2013.

Boyd, P. and Trull, T.: Understanding the export of biogenic particles in oceanic waters: Is there consensus?, Progress in Oceanography, 72, 276–312, https://doi.org/10.1016/j.pocean.2006.10.007, 2007.

Bratley, P. and Fox, B. L.: Algorithm 659: Implementing Sobol's quasirandom sequence generator, ACM Trans. Math. Softw., 14, 88–100, https://doi.org/10.1145/42288.214372, 1988.

Caron, D., Dam, H., Kremer, P., Lessard, E., Madin, L., Malone, T., Napp, J., Peele, E., Roman, M., and Youngbluth, M.: The contribution of microorganisms to particulate carbon and nitrogen in surface waters of the Sargasso Sea near Bermuda, Deep Sea Research Part I: Oceanographic Research Papers, 42, 943–972, https://doi.org/10.1016/0967-0637(95)00027-4, 1995.

Cavan, E. L., Henson, S. A., Belcher, A., and Sanders, R.: Role of zooplankton in determining the efficiency of the biological carbon pump, Biogeosciences, 14, 177–186, https://doi.org/10.5194/bg-14-177-2017, 2017.

Chen, B., Liu, H., and Lau, M.: Grazing and growth responses of a marine oligotrichous ciliate fed with two nanoplankton: Does food quality matter for micrograzers?, Aquatic Ecology, 44, 113–119, https://doi.org/10.1007/s10452-009-9264-5, 2010.

https://doi.org/10.5194/egusphere-2026-5134
Preprint. Discussion started: 8 September 2026

Christaki, U., Giannakourou, A., Van Wambeke, F., and Grégori, G.: Nanoflagellate predation on auto- and heterotrophic picoplankton in the oligotrophic Mediterranean Sea, Journal of plankton research, 23, 1297–1310, https://doi.org/10.1093/plankt/23.11.1297, 2001.

Christaki, U., Van Wambeke, F., Lefevre, D., Lagaria, A., Prieur, L., Pujo-Pay, M., Grattepanche, J.-D., Colombet, J., Psarra, S., Dolan, J. R., Sime-Ngando, T., Conan, P., Weinbauer, M. G., and Moutin, T.: Microbial food webs and metabolic state across oligotrophic waters of the Mediterranean Sea during summer, Biogeosciences, 8, 1839–1852, https://doi.org/10.5194/bg-8-1839-2011, 2011.

Ciavatta, S., Lazzari, P., Álvarez, E., Bertino, L., Bolding, K., Bruggeman, J., Capet, A., Cossarini, G., Daryabor, F., Nerger, L., Popov, M., Skákala, J., Spada, S., Teruzzi, A., Wakamatsu, T., Yumruktepe, V., and Brasseur, P.: Control of simulated ocean ecosystem indicators by biogeochemical observations, Progress in Oceanography, 231, 103 384, https://doi.org/10.1016/j.pocean.2024.103384, 2025.

Clavano, W., Boss, E., and Karp-Boss, L.: Inherent Optical Properties of Non-Spherical Marine-Like Particles – From Theory To Observation, vol. 45, pp. 1–38, ISBN 978-1-4200-5093-6, 2007.

Coppola, L., Diamond Riquier, E., Carval, T., Irisson, J.-O., and Desnos, C.: Dyfamed Observatory Data, https://doi.org/10.17882/43749, 2023.

Eddy, T. D., Heneghan, R. F., Bryndum-Buchholz, A., Fulton, E. A., Harrison, C. S., Tittensor, D. P., Lotze, H. K., Ortega-Cisneros, K., Novaglio, C., Bianchi, D., Büchner, M., Bulman, C., Cheung, W. W. L., Christensen, V., Coll, M., Everett, J. D., Fierro-Arcos, D., Galbraith, E. D., Gascuel, D., Guiet, J., Mackinson, S., Maury, O., Niiranen, S., Oliveros-Ramos, R., Palacios-Abrantes, J., Piroddi, C., du Pontavice, H., Reum, J., Richardson, A. J., Schewe, J., Shannon, L., Shin, Y.-J., Steenbeek, J., Volkholz, J., Walker, N. D., Woodworth-Jefcoats, P., and Blanchard, J. L.: Global and Regional Marine Ecosystem Models Reveal Key Uncertainties in Climate Change Projections, Earth's Future, 13, e2024EF005 537, https://doi.org/10.1029/2024EF005537, 2025.

Eiler, A., Langenheder, S., Bertilsson, S., and Tranvik, L. J.: Heterotrophic Bacterial Growth Efficiency and Community Structure at Different Natural Organic Carbon Concentrations, Applied and Environmental Microbiology, 69, 3701–3709, https://doi.org/10.1128/AEM.69.7.3701-3709.2003, 2003.

Fasham, M. J., Ducklow, H. W., and McKelvie, S. M.: A nitrogen-based model of plankton dynamics in the oceanic mixed layer, Journal of Marine Research, 48, https://elischolar.library.yale.edu/journal_of_marine_research/1981, 1990.

Faure, V., Pinazo, C., Torréton, J.-P., and Douillet, P.: Relevance of various formulations of phytoplankton chlorophyll *a*:carbon ratio in a 3D marine ecosystem model, Comptes Rendus. Biologies, 329, 813–822, https://doi.org/10.1016/j.crvi.2006.07.006, 2006.

Ferrari, S. and Cribari-Neto, F.: Beta Regression for Modelling Rates and Proportions, Journal of Applied Statistics, 31, 799–815, https://doi.org/10.1080/0266476042000214501, 2004.

Fiechter, J.: Assessing marine ecosystem model properties from ensemble calculations, Ecological Modelling, 242, 164–179, https://doi.org/10.1016/j.ecolmodel.2012.05.016, 2012.

Forrester, A. I., Sóbester, A., and Keane, A. J.: Multi-fidelity optimization via surrogate modelling, Proceedings of the Royal Society A: Mathematical, Physical and Engineering Sciences, 463, 3251–3269, https://doi.org/10.1098/rspa.2007.1900, 2007.

Geider, R. J.: LIGHT AND TEMPERATURE DEPENDENCE OF THE CARBON TO CHLOROPHYLL a RATIO IN MICROALGAE AND CYANOBACTERIA: IMPLICATIONS FOR PHYSIOLOGY AND GROWTH OF PHYTOPLANKTON, New Phytologist, 106, 1–34, https://doi.org/10.1111/j.1469-8137.1987.tb04788.x, 1987.

Geider, R. J. and La Roche, J.: Redfield revisited: variability of C:N:P in marine microalgae and its biochemical basis, European Journal of Phycology, 37, 1–17, https://doi.org/10.1017/S0967026201003456, 2002.

https://doi.org/10.5194/egusphere-2026-5134
Preprint. Discussion started: 8 September 2026

Giering, S., Sanders, R., Lampitt, R., Anderson, T., Tamburini, C., Boutrif, M., Zubkov, M., Marsay, C., Henson, S., Saw, K., Cook, K., and Mayor, D.: Reconciliation of the carbon budget in the ocean's twilight zone, Nature, 507, 480–3, https://doi.org/10.1038/nature13123, 2014.

Halsband-Lenk, C., Carlotti, F., and Greve, W.: Life-history strategies of calanoid congeners under two different climate regimes: a comparison, ICES Journal of Marine Science, 61, 709–720, https://doi.org/10.1016/j.icesjms.2004.03.020, 2004.

Hemmings, J. C. P., Challenor, P. G., and Yool, A.: Mechanistic site-based emulation of a global ocean biogeochemical model (MEDUSA 1.0) for parametric analysis and calibration: an application of the Marine Model Optimization Testbed (MarMOT 1.1), Geoscientific Model Development, 8, 697–731, https://doi.org/10.5194/gmd-8-697-2015, 2015.

IPCC: Climate Change 2023: Synthesis Report. *Contribution of Working Groups I, II and III to the Sixth Assessment Report of the Intergovernmental Panel on Climate Change*, Tech. rep., IPCC, Geneva, Switzerland, https://doi.org/10.59327/IPCC/AR6-9789291691647, 2023.

Irwin, A. J., Finkel, Z. V., Schofield, O. M. E., and Falkowski, P. G.: Scaling-up from nutrient physiology to the size-structure of phytoplankton communities, Journal of Plankton Research, 28, 459–471, https://doi.org/10.1093/plankt/fbi148, 2006.

Jacquet, S., Prieur, L., Avois-Jacquet, C., Lennon, J.-F., and Vaulot, D.: Short-timescale variability of picophytoplankton abundance and cellular parameters in surface waters of the Alboran Sea (western Mediterranean), Journal of Plankton Research, 24, 635–651, https://doi.org/10.1093/plankt/24.7.635, 2002.

Jordan, M. J., Klee, E. F., Hamlington, P. E., Lovenduski, N. S., and Niemeyer, K. E.: Automatic reduction of ocean biogeochemical models: a case study with BFM (v5.3), EGUsphere, 2025, 1–51, https://doi.org/10.5194/egusphere-2025-2901, 2025.

Kennedy, M. C. and O'Hagan, A.: Bayesian calibration of computer models, Journal of the Royal Statistical Society Series B, 63, 425–464, https://doi.org/10.1111/1467-9868.00294, 2001.

Kriest, I. and Oschlies, A.: On the treatment of particulate organic matter sinking in large-scale models of marine biogeochemical cycles, Biogeosciences, 5, 55–72, https://doi.org/10.5194/bg-5-55-2008, 2008.

Kruschke, J.: Doing Bayesian data analysis: A tutorial with R, JAGS, and Stan, second edition, https://doi.org/10.1016/B978-0-12-405888-0.09999-2, 2014.

Kulk, G., Platt, T., Dingle, J., Jackson, T., Jönsson, B. F., Bouman, H. A., Babin, M., Brewin, R. J. W., Doblin, M., Estrada, M., Figueiras, F. G., Furuya, K., González-Benítez, N., Gudfinnsson, H. G., Gudmundsson, K., Huang, B., Isada, T., Kovač, Ž., Lutz, V. A., Marañón, E., Raman, M., Richardson, K., Rozema, P. D., Poll, W. H. v. d., Segura, V., Tilstone, G. H., Uitz, J., Dongen-Vogels, V. v., Yoshikawa, T., and Sathyendranath, S.: Primary Production, an Index of Climate Change in the Ocean: Satellite-Based Estimates over Two Decades, Remote Sensing, 12, https://doi.org/10.3390/rs12050826, 2020.

La Ferla, R., Lo Giudice, A., and Maimone, G.: Morphology and LPS content for the estimation of marine bacterioplankton biomass in the Ionian Sea, Scientia Marina, 68, 23–31, https://doi.org/10.3989/scimar.2004.68n123, 2004.

Landry, M. R., Al-Mutairi, H., Selph, K. E., Christensen, S., and Nunnery, S.: Seasonal patterns of mesozooplankton abundance and biomass at Station ALOHA, Deep Sea Research Part II: Topical Studies in Oceanography, 48, 2037–2061, https://doi.org/10.1016/S0967-0645(00)00172-7, 2001.

Lazzari, P., Mattia, G., Solidoro, C., Salon, S., Crise, A., Zavatarelli, M., Oddo, P., and Vichi, M.: The impacts of climate change and environmental management policies on the trophic regimes in the Mediterranean Sea: Scenario analyses, Journal of Marine Systems, 135, 137–149, https://doi.org/10.1016/j.jmarsys.2013.06.005, 2014.

https://doi.org/10.5194/egusphere-2026-5134
Preprint. Discussion started: 8 September 2026

Le Roux, E., Tandeo, P., Granero Belinchon, C., Baklouti, M., Le Sommer, J., Sevault, F., Somot, S., Doury, A., and Al Najar, M.: Equation discovery for climate impact: emulating impact models for unexplored climate scenario with interpretable symbolic regression, EGUsphere, 2026, 1–27, https://doi.org/10.5194/egusphere-2026-1991, 2026.

Leblanc, K., Queguiner, B., Diaz, F., Cornet, V., Michel-Rodriguez, M., Durrieu de Madron, X., Bowler, C., Malviya, S., Thyssen, M., Grégori, G., et al.: Nanoplanktonic diatoms are globally overlooked but play a role in spring blooms and carbon export, Nature communications, 9, 953, https://doi.org/10.1038/s41467-018-03376-9, 2018.

Lee, S. and Fuhrman, J.: Relationships between Biovolume and Biomass of Naturally Derived Marine Bacterioplankton, Applied and environmental microbiology, 53, 1298—1303, https://doi.org/10.1128/aem.53.6.1298-1303.1987, 1987.

Leles, S. G., VaLEntin, J. L., and FiGuEirEdo, G. M.: Evaluation of the complexity and performance of marine planktonic trophic models, Anais da Academia Brasileira de Ciências, 88, 1971–1991, https://doi.org/10.1590/0001-3765201620150588, 2016.

Liefer, J. D., Garg, A., Fyfe, M. H., Irwin, A. J., Benner, I., Brown, C. M., Follows, M. J., Omta, A. W., and Finkel, Z. V.: The Macromolecular Basis of Phytoplankton C:N:P Under Nitrogen Starvation, Frontiers in Microbiology, Volume 10 - 2019, https://doi.org/10.3389/fmicb.2019.00763, 2019.

Löptien, U., Dietze, H., Preuss, R., and Toussaint, U.: Mapping manifestations of parametric uncertainty in projected pelagic oxygen concentrations back to contemporary local model fidelity, Scientific Reports, 11, https://doi.org/10.1038/s41598-021-00334-2, 2021.

Maimone, G., Azzaro, M., Placenti, F., Paranhos, R., Cabral, A. S., Decembrini, F., Zaccone, R., Cosenza, A., Rappazzo, A. C., Patti, B., Basilone, G., Cuttitta, A., Ferreri, R., Aronica, S., and Ferla, R. L.: A Morphometric Approach to Understand Prokaryoplankton: A Study in the Sicily Channel (Central Mediterranean Sea), Microorganisms, 11, https://doi.org/10.3390/microorganisms11041019, 2023.

Mamnun, N., Völker, C., Vrekoussis, M., and Nerger, L.: Uncertainties in ocean biogeochemical simulations: Application of ensemble data assimilation to a one-dimensional model, Frontiers in Marine Science, Volume 9 - 2022, https://doi.org/10.3389/fmars.2022.984236, 2022.

Mamnun, N., Völker, C., Krumscheid, S., Vrekoussis, M., and Nerger, L.: Global sensitivity analysis of a one-dimensional ocean biogeochemical model, Socio-Environmental Systems Modelling, 5, 18 613, https://doi.org/10.18174/sesmo.18613, 2023.

Marañón, E., Van Wambeke, F., Uitz, J., Boss, E. S., Dimier, C., Dinasquet, J., Engel, A., Haëntjens, N., Pérez-Lorenzo, M., Taillandier, V., and Zäncker, B.: Deep maxima of phytoplankton biomass, primary production and bacterial production in the Mediterranean Sea, Biogeosciences, 18, 1749–1767, https://doi.org/10.5194/bg-18-1749-2021, 2021.

Marino, S., Hogue, I. B., Ray, C. J., and Kirschner, D. E.: A methodology for performing global uncertainty and sensitivity analysis in systems biology, Journal of Theoretical Biology, 254, 178–196, https://doi.org/10.1016/j.jtbi.2008.04.011, 2008.

Massey, F. J.: The Kolmogorov-Smirnov Test for Goodness of Fit, Journal of the American Statistical Association, 46, 68–78, https://doi.org/10.2307/2280095, 1951.

Moore, J. K., Lindsay, K., Doney, S. C., Long, M. C., and Misumi, K.: Marine Ecosystem Dynamics and Biogeochemical Cycling in the Community Earth System Model [CESM1(BGC)]: Comparison of the 1990s with the 2090s under the RCP4.5 and RCP8.5 Scenarios, Journal of Climate, 26, 9291 – 9312, https://doi.org/10.1175/JCLI-D-12-00566.1, 2013.

Morell, A., Shin, Y.-J., Barrier, N., Travers-Trolet, M., Halouani, G., and Ernande, B.: Bioen-OSMOSE: A bioenergetic marine ecosystem model with physiological response to temperature and oxygen, Progress in Oceanography, 216, 103 064, https://doi.org/10.1016/j.pocean.2023.103064, 2023.

Murphy, J. M., Sexton, D. M., Barnett, D. N., Jones, G. S., Webb, M. J., Collins, M., and Stainforth, D. A.: Quantification of modelling uncertainties in a large ensemble of climate change simulations, Nature, 430, 768–772, https://doi.org/10.1038/nature02771, 2004.

https://doi.org/10.5194/egusphere-2026-5134
Preprint. Discussion started: 8 September 2026

Niemeyer, D., Kriest, I., and Oschlies, A.: The effect of marine aggregate parameterisations on nutrients and oxygen minimum zones in a global biogeochemical model, Biogeosciences, 16, 3095–3111, https://doi.org/10.5194/bg-16-3095-2019, 2019.

O'Neill, B. C., Tebaldi, C., van Vuuren, D. P., Eyring, V., Friedlingstein, P., Hurtt, G., Knutti, R., Kriegler, E., Lamarque, J.-F., Lowe, J., Meehl, G. A., Moss, R., Riahi, K., and Sanderson, B. M.: The Scenario Model Intercomparison Project (ScenarioMIP) for CMIP6, Geoscientific Model Development, 9, 3461–3482, https://doi.org/10.5194/gmd-9-3461-2016, 2016.

O'Hagan, A.: Bayesian analysis of computer code outputs: A tutorial, Reliability Engineering System Safety, 91, 1290–1300, https://doi.org/10.1016/j.ress.2005.11.025, 2006.

Pagès, R., Baklouti, M., Barrier, N., Ayache, M., Sevault, F., Somot, S., and Moutin, T.: Projected effects of climate-induced changes in hydrodynamics on the biogeochemistry of the Mediterranean Sea under the RCP 8.5 regional climate scenario, *Frontiers in Marine Science*, 7, 563 615, https://doi.org/10.3389/fmars.2020.563615, 2020.

Payne, M. R., Barange, M., Cheung, W. W. L., MacKenzie, B. R., Batchelder, H. P., Cormon, X., Eddy, T. D., Fernandes, J. A., Hollowed, A. B., Jones, M. C., Link, J. S., Neubauer, P., Ortiz, I., Queirós, A. M., and Paula, J. R.: Uncertainties in projecting climate-change impacts in marine ecosystems, ICES Journal of Marine Science, 73, 1272–1282, https://doi.org/10.1093/icesjms/fsv231, 2016.

Peherstorfer, B., Willcox, K., and Gunzburger, M.: Survey of Multifidelity Methods in Uncertainty Propagation, Inference, and Optimization, SIAM Review, 60, 550–591, https://doi.org/10.1137/16M1082469, 2018.

Percopo, I., Siano, R., Cerino, F., Sarno, D., and Zingone, A.: Phytoplankton diversity during the spring bloom in the northwestern Mediterranean Sea, Botanica Marina, 54, 243–267, https://doi.org/10.1515/BOT.2011.033, 2011.

Pianosi, F., Beven, K., Freer, J., Hall, J. W., Rougier, J., Stephenson, D. B., and Wagener, T.: Sensitivity analysis of environmental models: A systematic review with practical workflow, Environmental Modelling & Software, 79, 214–232, https://doi.org/10.1016/j.envsoft.2016.02.008, 2016.

Planque, B., Aarflot, J. M., Buttay, L., Carroll, J., Fransner, F., Hansen, C., Husson, B., Øystein Langangen, Lindstrøm, U., Pedersen, T., Primicerio, R., Sivel, E., Skogen, M. D., Strombom, E., Stige, L. C., Øystein Varpe, and Yoccoz, N. G.: A standard protocol for describing the evaluation of ecological models, Ecological Modelling, 471, 110 059, https://doi.org/10.1016/j.ecolmodel.2022.110059, 2022.

Prieur, C., Viry, L., Blayo, E., and Brankart, J.-M.: A global sensitivity analysis approach for marine biogeochemical modeling, Ocean Modelling, 139, 101 402, https://doi.org/10.1016/j.ocemod.2019.101402, 2019.

Pulido-Villena, E., Wagener, T., and Guieu, C.: Bacterial response to dust pulses in the western Mediterranean: Implications for carbon cycling in the oligotrophic ocean, Global Biogeochemical Cycles, 22, https://doi.org/10.1029/2007GB003091, 2008.

Pérez, M., Dolan, J., Vidussi, F., and Fukai, E.: Diel vertical distribution of planktonic ciliates within the surface layer of the NW Mediterranean (May 1995), Deep Sea Research Part I: Oceanographic Research Papers, 47, 479–503, https://doi.org/10.1016/S0967-0637(99)00099-0, 2000.

Quevedo, M. and Anadon, R.: Spring microzooplankton composition, biomass and potential grazing in the central Cantabrian coast (southern Bay of Biscay), Oceanologica Acta, 23, 297–310, https://doi.org/10.1016/S0399-1784(00)00128-6, 2000.

Quéré, C. L., Harrison, S. P., Colin Prentice, I., Buitenhuis, E. T., Aumont, O., Bopp, L., Claustre, H., Cotrim Da Cunha, L., Geider, R., Giraud, X., Klaas, C., Kohfeld, K. E., Legendre, L., Manizza, M., Platt, T., Rivkin, R. B., Sathyendranath, S., Uitz, J., Watson, A. J., and Wolf-Gladrow, D.: Ecosystem dynamics based on plankton functional types for global ocean biogeochemistry models, Global Change Biology, 11, 2016–2040, https://doi.org/10.1111/j.1365-2486.2005.1004.x, 2005.

Raick, C., Soetaert, K., and Grégoire, M.: Model complexity and performance: How far can we simplify?, Progress in Oceanography, 70, 27–57, https://doi.org/10.1016/j.pocean.2006.03.001, 2006.

https://doi.org/10.5194/egusphere-2026-5134
Preprint. Discussion started: 8 September 2026

Razavi, S., Tolson, B. A., and Burn, D. H.: Review of surrogate modeling in water resources, Water Resources Research, 48, https://doi.org/10.1029/2011WR011527, 2012.

Refsgaard, J. C., van der Sluijs, J. P., Brown, J., and van der Keur, P.: A framework for dealing with uncertainty due to model structure error, Advances in Water Resources, 29, 1586–1597, https://doi.org/10.1016/j.advwatres.2005.11.013, 2006.

Refsgaard, J. C., van der Sluijs, J. P., Højberg, A. L., and Vanrolleghem, P. A.: Uncertainty in the environmental modelling process – A framework and guidance, Environmental Modelling & Software, 22, 1543–1556, https://doi.org/10.1016/j.envsoft.2007.02.004, 2007.

Riahi, K., van Vuuren, D. P., Kriegler, E., Edmonds, J., O'Neill, B. C., Fujimori, S., Bauer, N., Calvin, K., Dellink, R., Fricko, O., Lutz, W., Popp, A., Cuaresma, J. C., KC, S., Leimbach, M., Jiang, L., Kram, T., Rao, S., Emmerling, J., Ebi, K., Hasegawa, T., Havlik, P., Humpenöder, F., Da Silva, L. A., Smith, S., Stehfest, E., Bosetti, V., Eom, J., Gernaat, D., Masui, T., Rogelj, J., Strefler, J., Drouet, L., Krey, V., Luderer, G., Harmsen, M., Takahashi, K., Baumstark, L., Doelman, J. C., Kainuma, M., Klimont, Z., Marangoni, G., Lotze-Campen, H., Obersteiner, M., Tabeau, A., and Tavoni, M.: The Shared Socioeconomic Pathways and their energy, land use, and greenhouse gas emissions implications: An overview, Global Environmental Change, 42, 153–168, https://doi.org/10.1016/j.gloenvcha.2016.05.009, 2017.

Richardson, A. J. and Verheye, H. M.: The relative importance of food and temperature to copepod egg production and somatic growth in the southern Benguela upwelling system, Journal of Plankton Research, 20, 2379–2399, https://doi.org/10.1093/plankt/20.12.2379, 1998.

Richardson, K., Bendtsen, J., Kragh, T., and Mousing, E. A.: Constraining the Distribution of Photosynthetic Parameters in the Global Ocean, Frontiers in Marine Science, Volume 3 - 2016, https://doi.org/10.3389/fmars.2016.00269, 2016.

Robinson, A., Bouman, H. A., Tilstone, G. H., and Sathyendranath, S.: Size Class Dependent Relationships between Temperature and Phytoplankton Photosynthesis-Irradiance Parameters in the Atlantic Ocean, Frontiers in Marine Science, Volume 4 - 2017, https://doi.org/10.3389/fmars.2017.00435, 2018.

Rose, K. A., Allen, J. I., Artioli, Y., Barange, M., Blackford, J., Carlotti, F., Cropp, R., Daewel, U., Edwards, K., Flynn, K., Hill, S. L., HilleRisLambers, R., Huse, G., Mackinson, S., Megrey, B., Moll, A., Rivkin, R., Salihoglu, B., Schrum, C., Shannon, L., Shin, Y., Smith, S. L., Smith, C., Solidoro, C., St. John, M., and Zhou, M.: End-To-End Models for the Analysis of Marine Ecosystems: Challenges, Issues, and Next Steps, Marine and Coastal Fisheries, 2, 115–130, https://doi.org/10.1577/C09-059.1, 2010.

Rumyantseva, A., Henson, S., Martin, A., Thompson, A. F., Damerell, G. M., Kaiser, J., and Heywood, K. J.: Phytoplankton spring bloom initiation: The impact of atmospheric forcing and light in the temperate North Atlantic Ocean, Progress in Oceanography, 178, 102 202, https://doi.org/10.1016/j.pocean.2019.102202, 2019.

Sacks, J., Welch, W. J., Mitchell, T. J., and Wynn, H. P.: Design and Analysis of Computer Experiments, Statistical Science, 4, 409 – 423, https://doi.org/10.1214/ss/1177012413, 1989.

Saillet, A.: Multi-Fidelity Gaussian Process Metamodeling: Application to the Eco3M-Med-CN Biogeochemical Model in a 1DV Configuration, Ph.D. thesis, Université Grenoble Alpes, phD thesis in preparation, in prep.

Saltelli, A., Tarantola, S., and Chan, K. P. S.: A Quantitative Model-Independent Method for Global Sensitivity Analysis of Model Output, Technometrics, 41, 39–56, https://doi.org/10.1080/00401706.1999.10485594, 1999.

Saltelli, A., Annoni, P., Azzini, I., Campolongo, F., Ratto, M., and Tarantola, S.: Variance based sensitivity analysis of model output. Design and estimator for the total sensitivity index, Computer Physics Communications, 181, 259–270, https://doi.org/10.1016/j.cpc.2009.09.018, 2010.

Sarrazin, F., Pianosi, F., and Wagener, T.: Global Sensitivity Analysis of environmental models: Convergence and validation, Environmental Modelling & Software, 79, 135–152, https://doi.org/10.1016/j.envsoft.2016.02.005, 2016.

https://doi.org/10.5194/egusphere-2026-5134
Preprint. Discussion started: 8 September 2026

Schartau, M., Wallhead, P., Hemmings, J., Löptien, U., Kriest, I., Krishna, S., Ward, B. A., Slawig, T., and Oschlies, A.: Reviews and syntheses: parameter identification in marine planktonic ecosystem modelling, Biogeosciences, 14, 1647–1701, https://doi.org/10.5194/bg-14-1647-2017, 2017.

Sempéré, R., Yoro, S. C., Van Wambeke, F., and Charrière, B.: Microbial decomposition of large organic particles in the northwestern Mediterranean Sea: an experimental approach, Marine Ecology Progress Series, 198, 61–72, https://doi.org/10.3354/meps198061, 2000.

Šimek, K., Macek, M., Pernthaler, J., Straškrabová, V., and Psenner, R.: Can freshwater planktonic ciliates survive on a diet of picoplankton?, Journal of Plankton Research, 18, 597–613, https://doi.org/10.1093/plankt/18.4.597, 1996.

Skákala, J., Awty-Carroll, K., Menon, P. P., Wang, K., and Lessin, G.: Future digital twins: emulating a highly complex marine biogeochemical model with machine learning to predict hypoxia, Frontiers in Marine Science, Volume 10 - 2023, https://doi.org/10.3389/fmars.2023.1058837, 2023.

Skákala, J., Ford, D., Fowler, A., Lea, D., Martin, M. J., and Ciavatta, S.: How uncertain and observable are marine ecosystem indicators in shelf seas?, Progress in Oceanography, 224, 103 249, https://doi.org/10.1016/j.pocean.2024.103249, 2024.

Smith, R. L., Tebaldi, C., Nychka, D., and Mearns, L. O.: Bayesian Modeling of Uncertainty in Ensembles of Climate Models, Journal of the American Statistical Association, 104, 97–116, https://doi.org/10.1198/jasa.2009.0007, 2009.

Sobol, I.: On the distribution of points in a cube and the approximate evaluation of integrals, USSR Computational Mathematics and Mathematical Physics, 7, 86–112, https://doi.org/10.1016/0041-5553(67)90144-9, 1967.

Steinberg, D. K. and Landry, M. R.: Zooplankton and the Ocean Carbon Cycle, Annual Review of Marine Science, 9, 413–444, https://doi.org/10.1146/annurev-marine-010814-015924, 2017.

Tanaka, T. and Rassoulzadegan, F.: Full-depth profile (0-2000m) of bacteria, heterotrophic nanoflagellates and ciliates in the NW Mediterranean Sea: Vertical partitioning of microbial trophic structures, Deep Sea Research Part II: Topical Studies in Oceanography, 49, 2093–2107, https://doi.org/10.1016/S0967-0645(02)00029-2, 2002.

Tanaka, T. and Rassoulzadegan, F.: Vertical and seasonal variations of bacterial abundance and production in the mesopelagic layer of the NW Mediterranean Sea: bottom-up and top-down controls, Deep Sea Research Part I: Oceanographic Research Papers, 51, 531–544, https://doi.org/10.1016/j.dsr.2003.12.001, 2004.

Trousselier, M., Bouvy, M., Courties, C., and Dupuy, C.: Variation of carbon content among bacterial species under starvation condition, Aquatic Microbial Ecology, https://doi.org/10.3354/ame013113, 1997.

Turley, M. C. and Ford, E. D.: Definition and calculation of uncertainty in ecological process models, Ecological Modelling, 220, 1968–1983, https://doi.org/10.1016/j.ecolmodel.2009.04.046, 2009.

Verity, P. G., Wassmann, P., Ratkova, T. N., Andreassen, I. J., Nordby, E., and Høisæter, T.: Seasonal patterns in composition and biomass of autotrophic and heterotrophic nano- and microplankton communities on the north Norwegian shelf, Sarsia, 84, 265–277, https://doi.org/10.1080/00364827.1999.10420431, 1999.

Vázquez-Domínguez, E., Duarte, C. M., Agustí, S., Jürgens, K., Vaqué, D., and Gasol, J. M.: Microbial plankton abundance and heterotrophic activity across the Central Atlantic Ocean, Progress in Oceanography, 79, 83–94, https://doi.org/10.1016/j.pocean.2008.08.002, 2008.

Wang, B. and Fennel, K.: Distinct sources of uncertainty in simulations of the ocean biological carbon pump at different depths, Communications Earth & Environment, 5, 395, https://doi.org/10.1038/s43247-024-01561-x, 2024.

Ward, B. A., Schartau, M., Oschlies, A., Martin, A. P., Follows, M. J., and Anderson, T. R.: When is a biogeochemical model too complex? Objective model reduction and selection for North Atlantic time-series sites, Progress in Oceanography, 116, 49–65, https://doi.org/10.1016/j.pocean.2013.06.002, 2013.

https://doi.org/10.5194/egusphere-2026-5134
Preprint. Discussion started: 8 September 2026

Zhang, Y., Baklouti, M., Brasseur, P., and Debreu, L.: A semi-automated sensitivity-based approach for simplifying marine biogeochemical models for targeted applications: A case study with the Eco3M-MED model, Ecological Modelling, 514, 111 491, https://doi.org/10.1016/j.ecolmodel.2026.111491, 2026.